


2008

# Light-trapping enhancement in thin film solar cells with photonic crystals

Dayu Zhou  
*Iowa State University*

Follow this and additional works at: <https://lib.dr.iastate.edu/rtd>

 Part of the [Electrical and Electronics Commons](#), [Energy Systems Commons](#), [Oil, Gas, and Energy Commons](#), and the [Power and Energy Commons](#)

## Recommended Citation

Zhou, Dayu, "Light-trapping enhancement in thin film solar cells with photonic crystals" (2008). *Retrospective Theses and Dissertations*. 15473.  
<https://lib.dr.iastate.edu/rtd/15473>

This Thesis is brought to you for free and open access by the Iowa State University Capstones, Theses and Dissertations at Iowa State University Digital Repository. It has been accepted for inclusion in Retrospective Theses and Dissertations by an authorized administrator of Iowa State University Digital Repository. For more information, please contact [digirep@iastate.edu](mailto:digirep@iastate.edu).

**Light-trapping enhancement in thin film solar cells  
with photonic crystals**

by

Dayu Zhou

A thesis submitted to the graduate faculty  
in partial fulfillment of the requirements for the degree of  
MASTER OF SCIENCE

Major: Electrical Engineering

Program of Study Committee:  
Rana Biswas, Major Professor  
Gary Tuttle  
Vikram Dalal  
Jiming Song

Iowa State University

Ames, Iowa

2008

Copyright © Dayu Zhou, 2008. All rights reserved.

UMI Number: 1454666

### INFORMATION TO USERS

The quality of this reproduction is dependent upon the quality of the copy submitted. Broken or indistinct print, colored or poor quality illustrations and photographs, print bleed-through, substandard margins, and improper alignment can adversely affect reproduction.

In the unlikely event that the author did not send a complete manuscript and there are missing pages, these will be noted. Also, if unauthorized copyright material had to be removed, a note will indicate the deletion.



---

UMI Microform 1454666  
Copyright 2008 by ProQuest LLC  
All rights reserved. This microform edition is protected against  
unauthorized copying under Title 17, United States Code.

---

ProQuest LLC  
789 East Eisenhower Parkway  
P.O. Box 1346  
Ann Arbor, MI 48106-1346

## DEDICATION

I would like to dedicate this thesis to my wife Xi for her everlasting love and support. I would also like to thank my friends and family for their loving guidance and financial assistance during the writing of this work.

## TABLE OF CONTENTS

<b>LIST OF FIGURES</b> . . . . .	v
<b>ABSTRACT</b> . . . . .	viii
<b>CHAPTER 1 GENERAL INTRODUCTION</b> . . . . .	1
Thin Film Solar Cells . . . . .	1
Photonic Crystals . . . . .	3
DBR . . . . .	6
2D Photonic Crystal Slab . . . . .	9
Scattering Matrix Method . . . . .	12
Thesis Organization . . . . .	15
References . . . . .	16
<b>CHAPTER 2 ENHANCING AND EFFICIENCY OF SOLAR CELLS WITH PHOTONIC CRYSTALS</b> . . . . .	17
Abstract . . . . .	17
Introduction . . . . .	18
Background . . . . .	18
Theoretical Model . . . . .	19
Light-trapping Schemes . . . . .	20
Simulation and Results . . . . .	22
Conclusions . . . . .	25
Acknowledgements . . . . .	25
References . . . . .	25

<b>CHAPTER 3 PHOTONIC CRYSTAL ENHANCED LIGHT-TRAPPING</b>	
<b>IN THIN FILM SOLAR CELLS</b> . . . . .	27
Abstract . . . . .	27
Introduction . . . . .	28
Light-trapping Schemes . . . . .	29
Simulation and Results . . . . .	31
Discussion and Conclusions . . . . .	37
Acknowledgements . . . . .	39
References . . . . .	39
<b>CHAPTER 4 GENERAL CONCLUSIONS</b> . . . . .	41
General Discussion . . . . .	41
Recommendations for Future Research . . . . .	42
References . . . . .	43
<b>ACKNOWLEDGEMENTS</b> . . . . .	45

## LIST OF FIGURES

Figure 1.1	a) The schematics of a p-i-n junction solar cell. b) The band diagram of a p-i-n junction solar cell . . . . .	2
Figure 1.2	The schematics of photonic crystals with periodicity in one, two and three dimensions. . . . .	4
Figure 1.3	The short circuit current ( $J_{sc}$ ) and the solar cell efficiency ( $\eta$ ) for p-i-n solar cell with 500 nm intrinsic layer thickness. a) AMPS simulation results with various p-layer thicknesses. b) AMPS simulation results with various n-layer. . . . .	6
Figure 1.4	a) The schematics of 10-layer DBR with definitions for design parameters and polarizations. b) Photonic band diagram for the DBR. . . . .	7
Figure 1.5	The reflectance from the 6-layer DBR for TE polarization at different angles, showing excellent agreement with scattering matrix simulations. . . . .	9
Figure 1.6	The angular dependency of the reflectance from the 30-layer DBR for both polarizations. The photonic bandgaps change with incident angles. . . . .	10
Figure 1.7	a) The reflection, transmission and absorption of 6-layer SiO <sub>2</sub> /Si DBR at normal incidence. b) The reflection, transmission and absorption of 10-layer ITO/Si DBR at normal incidence. . . . .	11
Figure 1.8	a) 2D photonic crystal structure with square lattice of cylinders in a dielectric slab. b) 2D photonic crystal structure with square lattice of cylinders in a dielectric slab. . . . .	11
Figure 1.9	The schematics of the incident wave and reflected wave from the 2D square lattice photonic crystal slab. . . . .	12

Figure 1.10	Definition of S matrix for photonic crystal slab with n layers. b) Definition of S matrix for an individual layer. . . . .	13
Figure 2.1	Energy dependent dielectric functions for a-Si:H with $E_g = 1.6$ eV, determined from spectroscopic ellipsometry by Ferlauto et al (Ref [10]).	20
Figure 2.2	Absorption length of photons as a function of wavelength for a-Si:H with $E_g = 1.6$ eV. The wavelength corresponding to the band edge $E_g$ is indicated by the arrow. . . . .	20
Figure 2.3	(a) Schematic solar cell configuration with antireflective coating, two-dimensional photonic crystal and distributed Bragg reflector (DBR) (b) Top view of 2D photonic crystal grating layer with amorphous silicon cylinders in $\text{SiO}_2$ background . . . . .	21
Figure 2.4	Reflection and transmission through 6-layer c-Si/ $\text{SiO}_2$ DBR for normal incidence . . . . .	22
Figure 2.5	Comparison of specular (S) and non-specular (NS) reflection from the 2D photonic crystal for different $R/a$ with $a = 0.70 \mu\text{m}$ , $d_3 = 0.04 \mu\text{m}$ and $d_4 = 300 \mu\text{m}$ . . . . .	23
Figure 2.6	Non-specular (total) reflection/transmission/absorption in the absorber layers for the two competing designs with $d_0 = 65 \text{ nm}$ , $d_1 = 50 \text{ nm}$ , $d_2 = 500 \text{ nm}$ and $d_2 = 120 \text{ nm}$ (a) a-Si layer with $\text{SiO}_2$ cylinders (b) $\text{SiO}_2$ layer with a-Si cylinders . . . . .	23
Figure 2.7	Comparison of absorption of a bare a-Si:H film, a-Si:H film with AR coating only, a-Si:H film with AR coating and DBR and the optimized solar cell with photonic crystal grating. . . . .	24
Figure 3.1	Absorption length of photons as a function of wavelength for a-Si:H with bandgap $E_g = 1.6$ eV. The bandgap wavelength is indicated by the arrow. . . . .	29



Figure 3.2	(a) Schematic solar cell configuration with top ITO, 2D PC, bottom ITO and DBR. (b) Top view of 2D PC grating layer with a-Si:H cylinders in an ITO background. . . . .	30
Figure 3.3	(Fourier component of the dielectric function and filling ratio, for the first reciprocal lattice vector $G_1 = 2\pi/a$ . . . . .	32
Figure 3.4	a) The variation in average absorption with thickness of the photonic crystal ( $d_3$ ), holding other parameters constant near the optimum values. b) The average absorption as a function of $d_6$ , for several values of the grating depth $d_3$ . . . . .	34
Figure 3.5	The variation in average absorption with lattice spacing 'a' of the photonic crystal, holding other parameters constant near the optimum values. . . . .	35
Figure 3.6	The variation in average absorption with cylinder radius of the photonic crystal, holding other parameters constant near the optimum values. . . . .	35
Figure 3.7	(a) The absorption of the optimized photonic crystal enhanced solar cell structure as a function of the wavelength, compared to the reference cell with antireflective coating and DBR only. (b) The absorption enhancement ratio of the optimized solar cell over the reference cell without the photonic crystal. (c) The ratio of the optical path length to the absorber layer thickness, for the optimized PC enhanced solar cell (solid) compared to the reference cell (dotted). The horizontal dashed line shows the theoretical limit of path length enhancement from a randomly roughened back reflector ( $\sim 50$ ). . . . .	36
Figure 4.1	a) The absorption and b) The diffraction in the gold nanoparticle array with $a = 1 \mu m$ , $d = 60 nm$ and $R/a$ of 0.05, 0.07, 0.09 and 0.11. . . . .	43

## ABSTRACT

Photovoltaics (or solar cell) has been an active area for research and development, driven by the world's constantly increasing needs for power. Among the current solar technologies, thin film solar cell promises lower cost, but at the expense of lower power conversion efficiency. The efficiency of thin film solar cell can be improved using light confinement schemes commonly referred to as light-trapping. In this thesis, we develop novel light-trapping schemes utilizing photonic crystals (PCs). The optical modeling is performed with a rigorous scattering matrix approach, where Maxwell's equations are solved in Fourier space, and simulations are carried out on parallel computation environment. Although the concepts apply to any thin film solar cell structures, hydrogenated amorphous silicon (a-Si:H) single junction thin film solar cell is used for simulation due to widely available optical property data.

In the solar cell structure we design, a one dimensional (1D) photonic crystal or distributed Bragg reflector (DBR) is used as back reflector. The DBR consists of alternating layers of  $\text{SiO}_2$  and Si or Indium Tin Oxide (ITO) and Si to provide high reflectivity with little loss. A layer of two dimensional (2D) photonic crystal slab between the a-Si:H absorber layer and the DBR can diffract light at oblique angles, so that total internal reflection can occur inside the absorber layer. The light path length inside the absorber layer will be greatly increased, so will the absorption. The parameters for photonic crystals are optimized through computer simulations to obtain the maximum absorption and path length enhancement. The simulations show significantly enhanced photon harvesting between 600 – 775 nm below the band edge. The path length enhancement can reach several hundred at resonant peaks, far exceeding the classical limit predicted for randomly roughened scattering surfaces.

## CHAPTER 1 GENERAL INTRODUCTION

### Thin Film Solar Cells

Thin film solar cells are usually produced by physical or chemical deposition techniques, which can be easily applied to large areas and fast throughput. Thin film technology is of much commercial interests because it offers lower costs and possibilities for mass production and deployment. Among all the thin film materials, amorphous silicon is the most developed one, and has been in commercial production since 1980 [1]. We choose a-Si:H as prototype material for this study due to better understanding of the material properties and widely available optical data.

The basic a-Si:H solar cell structure is p-i-n junction shown in figure 1.1a. The minority carrier diffusion length in undoped a-Si:H is typically around  $0.1 \mu m$  [1], so an electric field needs to be created in the intrinsic layer to separate and collect the photo-generated electron-hole pairs. The p-i-n solar cell should be designed such that the depletion width is greater than the intrinsic layer thickness and the built-in electric field is across the entire intrinsic layer (Fig. 1.1b). For this reason, the thickness of the intrinsic layer in a p-i-n structure is limited to around  $500 nm$ . The small amount of material used in amorphous silicon solar cells lower the cost substantially. In contrast a large amount of material ( $> 10 \mu m$  in thickness) is needed for crystalline silicon solar cells where the optical absorption is much weaker.

Light trapping is the standard technique for improving the thin film solar cell efficiencies and for harvesting the spectrum of incoming sunlight. Since amorphous silicon and most common semiconductor materials have a high refractive index at optical wavelengths, considerable amount of light is reflected from the top surface of the film. The first optical enhancement technique commonly used is to employ an anti-reflective coating layer placed on the top of the

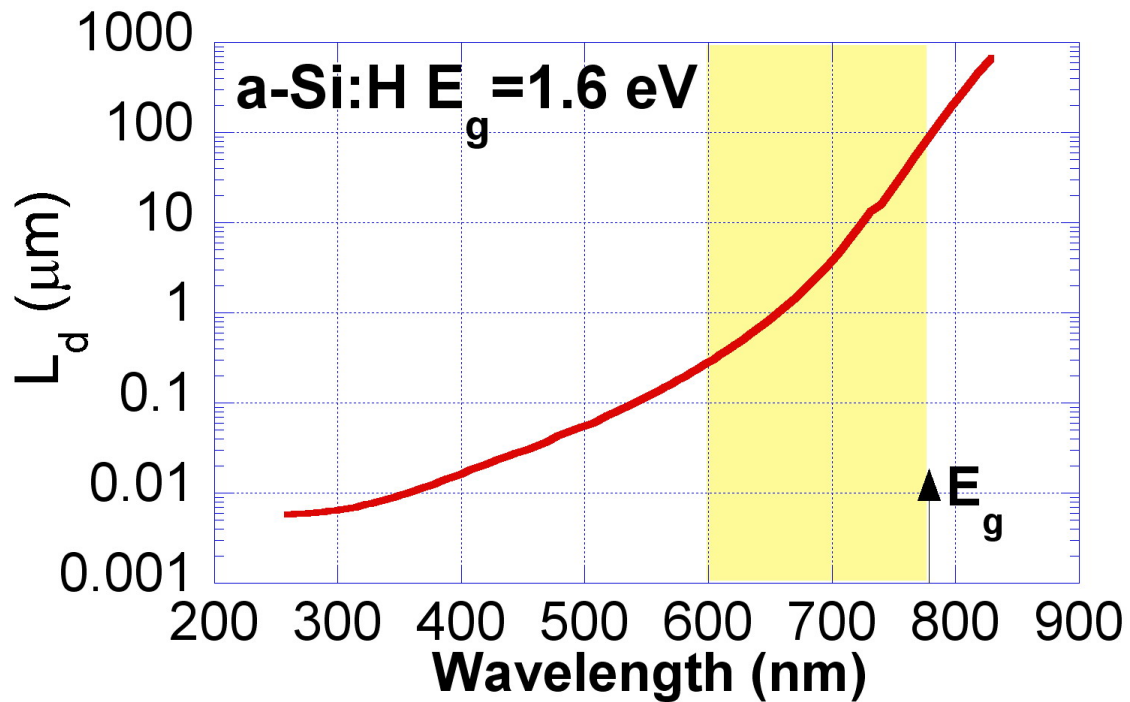


Figure 1.1 a) The schematics of a p-i-n junction solar cell. b) The band diagram of a p-i-n junction solar cell

solar cell absorber layer. The thickness of the coating is approximately quarter wavelength inside the dielectric, so that the reflected waves will interference destructively. In state-of-the-art solar cells, and in our simulation, ITO is used as both anti-reflective coating and top contact for the solar cell.

The second optical enhancement technique is to use a high reflectivity mirror at the back that will prevent the light escaping from the rear surface and double the light path. The rear surface is typically metalized with aluminum or silver and can provide reflectivity of over 95%. However two optical passes are not adequate to absorb photons with large absorption lengths and a critical technique is light-trapping where the optical path length or photon dwell-time is increases within the absorber layer. The common light-trapping technique in solar cells is to utilize a textured back reflector to reflect the incoming light at an oblique angle. As long as the light can deviate from the normal direction larger than the critical angle, total internal reflection can occur at the top surface and the light path can be further increased. In the case

the amorphous silicon, the critical angle is around  $14^\circ$ .

A perfect randomly roughened back surface (a Lambertian surface) can reflect light into all angles with equal possibility. For this ideal surface, the predicted path length enhancement is  $4n^2$  times the thickness of the solar cell, where  $n$  is the refractive index of the semiconductor, corresponding to around 50 in silicon [2]. A popular texturing scheme is using roughened silver reflectors coated with ZnO [3]. Such textured metallic reflectors suffer from intrinsic losses from surface plasmon modes generated at the granular metal-dielectric interface. Such losses can be 3% to 8% with each light pass at 650 nm for different surface roughness [3] and can accumulate rapidly and become even more severe at longer wavelengths. For example in the regime of long absorption lengths a loss of  $L$  with each reflection can lead to a loss of  $1 - (1 - L)^n$  with  $n$  passes. For  $L = 5\%$ , 40% of the light is lost in 10 passes, which is a considerable loss. So in reality, the best light path enhancement is a little over 10 times the cell thickness [1], much smaller than the theoretical limit.

## Photonic Crystals

Since photonic crystals are used extensively in this thesis to enhance light-trapping in solar cells, we provide a brief summary of photonic crystal properties. Photonic crystals are artificial materials with periodic dielectric constants in one, two or three dimensions, as shown in figure 1.2 [5]. With careful designs, photonic crystals can exhibit photonic band gaps, so that electromagnetic waves of certain frequency range cannot propagate along specific direction inside.

The propagation of electromagnetic waves inside photonic crystal structures is governed by the four macroscopic Maxwell's equations:

$$\begin{aligned} \nabla \cdot \mathbf{B} &= 0, & \nabla \times \mathbf{E} + \frac{\partial \mathbf{B}}{\partial t} &= 0 \\ \nabla \cdot \mathbf{D} &= \rho, & \nabla \times \mathbf{H} - \frac{\partial \mathbf{D}}{\partial t} &= \mathbf{J} \end{aligned} \quad (1.1)$$

where  $\mathbf{E}$  and  $\mathbf{B}$  are the macroscopic electric and magnetic fields quantities,  $\mathbf{D}$  and  $\mathbf{H}$  are

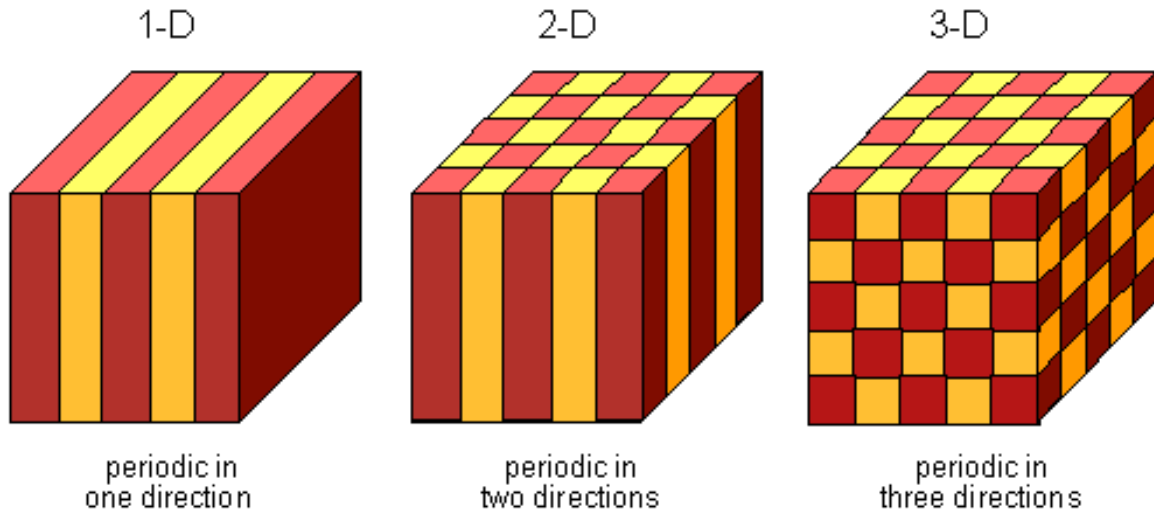


Figure 1.2 The schematics of photonic crystals with periodicity in one, two and three dimensions.

corresponding derived fields. In general, there is no free charge or current, so

$$\rho = \mathbf{J} = 0 \quad (1.2)$$

In linear isotropic materials, the constitutive relation gives:

$$\mathbf{D}(\mathbf{r}, \omega) = \epsilon(\mathbf{r}, \omega) \mathbf{E}(\mathbf{r}, \omega) \quad \mathbf{B}(\mathbf{r}, \omega) = \mu \mathbf{H}(\mathbf{r}, \omega) \quad (1.3)$$

In general,  $\epsilon$  is a frequency dependent complex valued function, which is also a periodic function of position, and  $\mu$  is a constant. The complex dielectric function accounts for absorption. The dielectric function changes appreciably within the frequency range we interested in, so we can not ignore the dispersion. With these assumptions, equation 1.1 becomes:

$$\nabla \times \mathbf{E}(\mathbf{r}, t) = -\mu \frac{\partial \mathbf{H}(\mathbf{r}, t)}{\partial t} \quad \nabla \times \mathbf{H}(\mathbf{r}, t) = \epsilon(\mathbf{r}) \frac{\partial \mathbf{E}(\mathbf{r}, t)}{\partial t} \quad (1.4)$$

In terms of time harmonics:

$$\nabla \times \mathbf{E}(\mathbf{r}) - j\omega\mu \mathbf{H}(\mathbf{r}) = 0 \quad \nabla \times \mathbf{H}(\mathbf{r}) + j\omega\epsilon(\mathbf{r}) \mathbf{E}(\mathbf{r}) = 0 \quad (1.5)$$

Combining the two equations in 1.5,

$$\nabla \times \left( \frac{1}{\epsilon(\mathbf{r})} \nabla \times \mathbf{H}(\mathbf{r}) \right) = \left( \frac{\omega}{c} \right)^2 \mathbf{H}(\mathbf{r}) \quad (1.6)$$

where  $c = 1/(\epsilon\mu)$ .

Equation 1.6 is essentially an eigenvalue problem with eigen operator  $\Theta$ ,

$$\Theta \equiv \nabla \times \left( \frac{1}{\epsilon(\mathbf{r})} \nabla \times \right) \quad (1.7)$$

and eigenvalue of  $(\omega/c)^2$ . The solutions of eigenfunction typically have to be obtained with computer simulations.

One of the most important implications of equation 1.6 is the scaling property. Suppose we scale the photonic crystal structure by a factor of  $s$ , so that,

$$\epsilon'(\mathbf{r}) = \epsilon(\mathbf{r}/s) \quad (1.8)$$

Then make a change of variable with  $\mathbf{r}' = s\mathbf{r}$  and  $\nabla' = \nabla/s$ , equation 1.6 becomes,

$$\nabla' \times \left( \frac{1}{\epsilon'(\mathbf{r}')} \nabla' \times \mathbf{H}(\mathbf{r}'/s) \right) = \left( \frac{\omega}{cs} \right)^2 \mathbf{H}(\mathbf{r}'/s) \quad (1.9)$$

We get the same equation as 1.6 with eigenvector  $\mathbf{H}'(\mathbf{r}) = \mathbf{H}(\mathbf{r}'/s)$  and eigenvalue  $\omega' = \omega/s$ . In other words, after scaling the structure by a factor of  $s$ , both the frequency and the field profile are scaled by the same factor. So in designing photonic crystals, the wavelengths of certain features can be controlled by adjusting the lattice constants of the photonic crystals. Another design rule of thumb is that the higher the dielectric constant contrast, the wider the bandgap. So we should use high dielectric contrast whenever possible.

One of the primary thrusts in the thesis is to replace the metallic back-reflector by a diffracting surface such as a photonic crystal. Photonic crystals made of dielectric material do not suffer from loss and will diffract light with the absorber layer, leading to enhancement of photon path length. Only the carriers generated in the intrinsic layer can be collected and contribute to the photo-current. The absorption occurred elsewhere will be lost. Since the light is coming from the p-layer, the p-layer thickness can strongly affect the performance of the solar cell. Analysis of Microelectronic and Photonic Structures (AMPS) simulations with 500 nm i-layer thickness show that both the short circuit current ( $J_{sc}$ ) and the solar cell efficiency ( $\eta$ ) degrade with increasing p-layer thickness rapidly (Fig. 1.3a). At the same time,  $J_{sc}$  and  $\eta$  do not change much with different n-layer thickness (Fig. 1.3b). For these reasons, it is

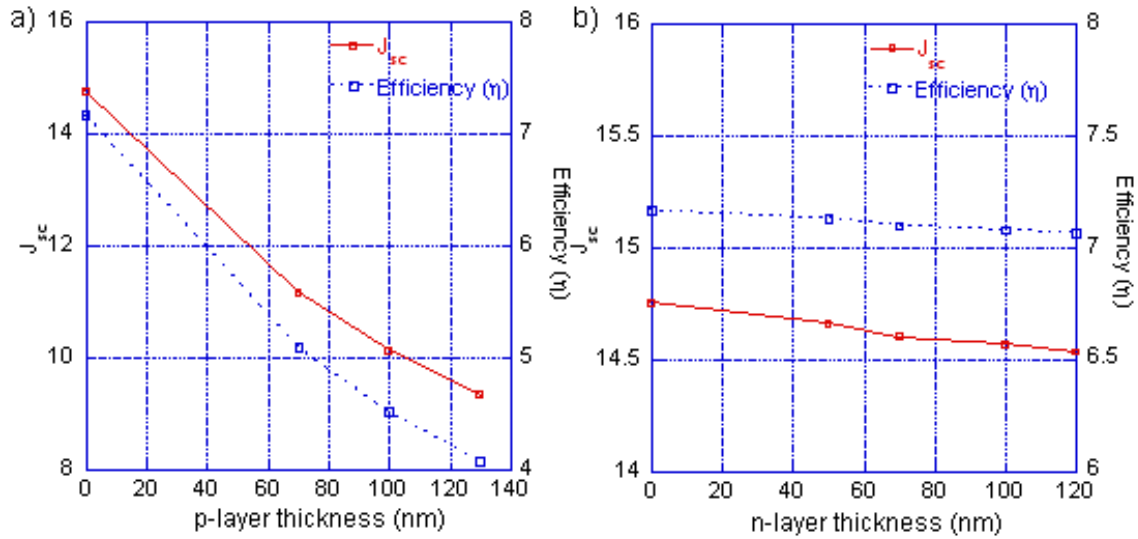


Figure 1.3 The short circuit current ( $J_{sc}$ ) and the solar cell efficiency ( $\eta$ ) for p-i-n solar cell with 500 nm intrinsic layer thickness. a) AMPS simulation results with various p-layer thicknesses. b) AMPS simulation results with various n-layer.

preferable to have the diffraction grating layer behind the n-layer instead of in front of the p-layer.

## DBR

The simplest photonic crystal is the one dimensional photonic crystal commonly known as Distributed Bragg Reflector (DBR). A 10-layer DBR is schematically shown in figure 1.4a, with definition of design parameters and polarizations. The solutions of equation 1.6 will give rise to dispersion relationship (photonic band diagram) for the DBR (Fig. 1.4b). Clearly, a photonic band gap is formed inside the DBR.

Generally, the width of the band gap varies with incident angles and polarizations. As the incident angles increase from zero to oblique angles, the bandgap for TE modes increase, whereas the bandgap for TM modes decrease. Nonetheless, there exists an omni-directional bandgap that is independent of angles and polarizations. The analytical expressions for the



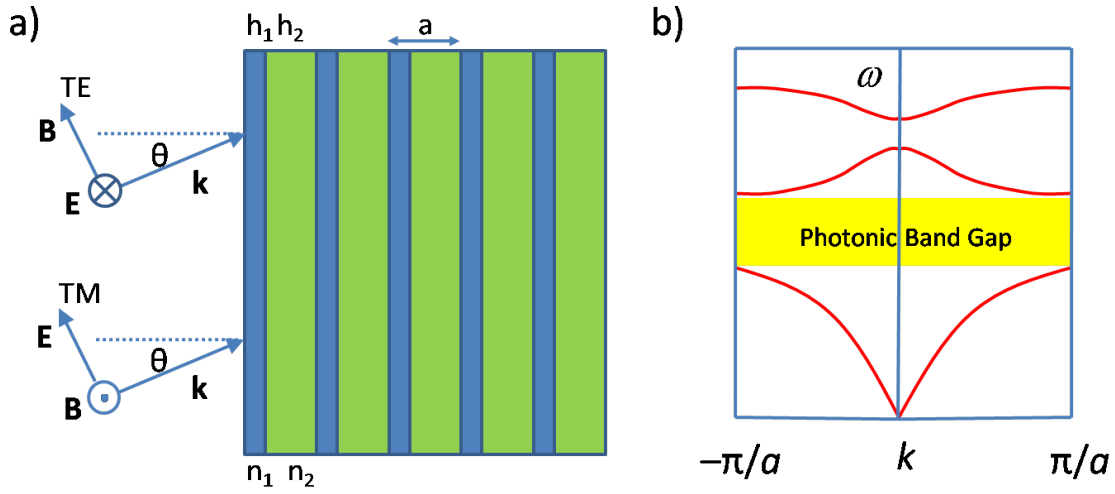


Figure 1.4 a) The schematics of 10-layer DBR with definitions for design parameters and polarizations. b) Photonic band diagram for the DBR.

band edges are given by [6],

$$\omega_h = \frac{2c}{h_2 n_2 + h_1 n_1} \arccos \left( - \left| \frac{n_1 - n_2}{n_1 + n_2} \right| \right) \quad (1.10)$$

$$\omega_l = \frac{2c}{h_2 \sqrt{n_2^2 - n_0^2} + h_1 \sqrt{n_1^2 - n_0^2}} \arccos \left( \left| \frac{n_1^2 \sqrt{n_2^2 - n_0^2} - n_2^2 \sqrt{n_1^2 - n_0^2}}{n_1^2 \sqrt{n_2^2 - n_0^2} + n_2^2 \sqrt{n_1^2 - n_0^2}} \right| \right) \quad (1.11)$$

DBR can be realized by quarter wavelength stacks of two dielectric materials. As long as there is a difference in dielectric constants, there will be a bandgap. Of course, the higher the contrast is, the wider the bandgap. Silicon ( $n_1 \sim 3.8$ ) and  $\text{SiO}_2$  ( $n_2 = 1.46$ ) stacks present an economical way of making the DBR. With  $h_1 = 50 \text{ nm}$  and  $h_2 = 120 \text{ nm}$ , an omni-directional bandgap can be obtained from equations 1.10 and 1.11 to be from 565 to 778 nm.

In reality, silicon is absorptive and dispersive, so frequency dependent complex valued dielectric constants have to be used in calculating the reflection and transmission through the DBR. In addition to the scattering matrix simulation program, analytical solutions to the Maxwell's equations can be obtained and implemented in Matlab.

The incident, reflected and transmitted fields can be formulated as  $2 \times 2$  matrix for a thin

film on a substrate [7],

$$\begin{bmatrix} F_i \\ F_r \end{bmatrix} = \frac{1}{2} \begin{bmatrix} 1 & 1/\kappa_i \\ 1 & -1/\kappa_i \end{bmatrix} \times \frac{1}{2} \begin{bmatrix} e^{-j\delta} + e^{j\delta} & (e^{-j\delta} - e^{j\delta})/\kappa_f \\ (e^{-j\delta} - e^{j\delta})\kappa_f & e^{-j\delta} + e^{j\delta} \end{bmatrix} \times \begin{bmatrix} 1 \\ \kappa_s \end{bmatrix} F_t \quad (1.12)$$

where  $\delta = kf, normd$  and  $d$  is the thickness of the film.  $k_{norm}$  is the normal component of the wave vector and generally a complex quantity. For TE polarization,  $F$  represents  $\mathbf{E}$  and  $\kappa = k_{norm}$ . For TM polarization,  $F$  represents  $\mathbf{H}$  and  $\kappa = k_{norm}/\epsilon$ . In the right hand side of equation 1.12, the first term corresponds to the input regain and the third term substrate. The second term can be defined as the transmittance matrix. For M layers, the individual transmittance matrix for each layer can be multiplied to obtain the total transmittance matrix,

$$\begin{bmatrix} F_i \\ F_r \end{bmatrix} = \frac{1}{2} \begin{bmatrix} 1 & 1/\kappa_i \\ 1 & -1/\kappa_i \end{bmatrix} \prod_{p=1}^M \left( \frac{1}{2} \begin{bmatrix} e^{-j\delta_p} + e^{j\delta_p} & (e^{-j\delta_p} - e^{j\delta_p})/\kappa_{f,p} \\ (e^{-j\delta_p} - e^{j\delta_p})\kappa_{f,p} & e^{-j\delta_p} + e^{j\delta_p} \end{bmatrix} \right) \begin{bmatrix} 1 \\ \kappa_s \end{bmatrix} F_t \quad (1.13)$$

These analytical solutions using equation 1.13 perfectly agree with the scattering matrix simulations. For 6-layer DBR consisting of silicon and SiO<sub>2</sub>, the results are shown below for TE polarization with incident angles of 0, 30, 60 and 89 degrees (Fig. 1.5).

To demonstrate the shifting of the band edges with increasing angles, the reflectance of 30-layer DBR has been calculated for both polarizations. In figure 1.6, the band edges are well defined in the 30-layer DBR. We observe the blue shift of long wavelength edges (low frequency edges), especially for TM modes. The omni-directional bandgap of the DBR is the overlap of the bandgaps for all the incident angles with both polarizations. In this case of a 30-layer DBR, the band edges are well predicted by equation 1.10 and 1.11, despite of the absorption and dispersion of the material.

For wavelengths less than the lower band edge (high frequency), the DBR is quite absorptive (Fig. 1.7). But this will not be a problem for solar cell back reflectors, as the higher energy photons can be completely absorbed by the intrinsic layer of the a-Si:H solar cell before they reach the DBR back reflector.

Another alternative DBR design involves using ITO and heavily doped poly-silicon. The benefit of this design is that the back reflector can be made conductive, thus eliminate the use of separate contact for the insulator DBR, which can be difficult to make. The dielectric

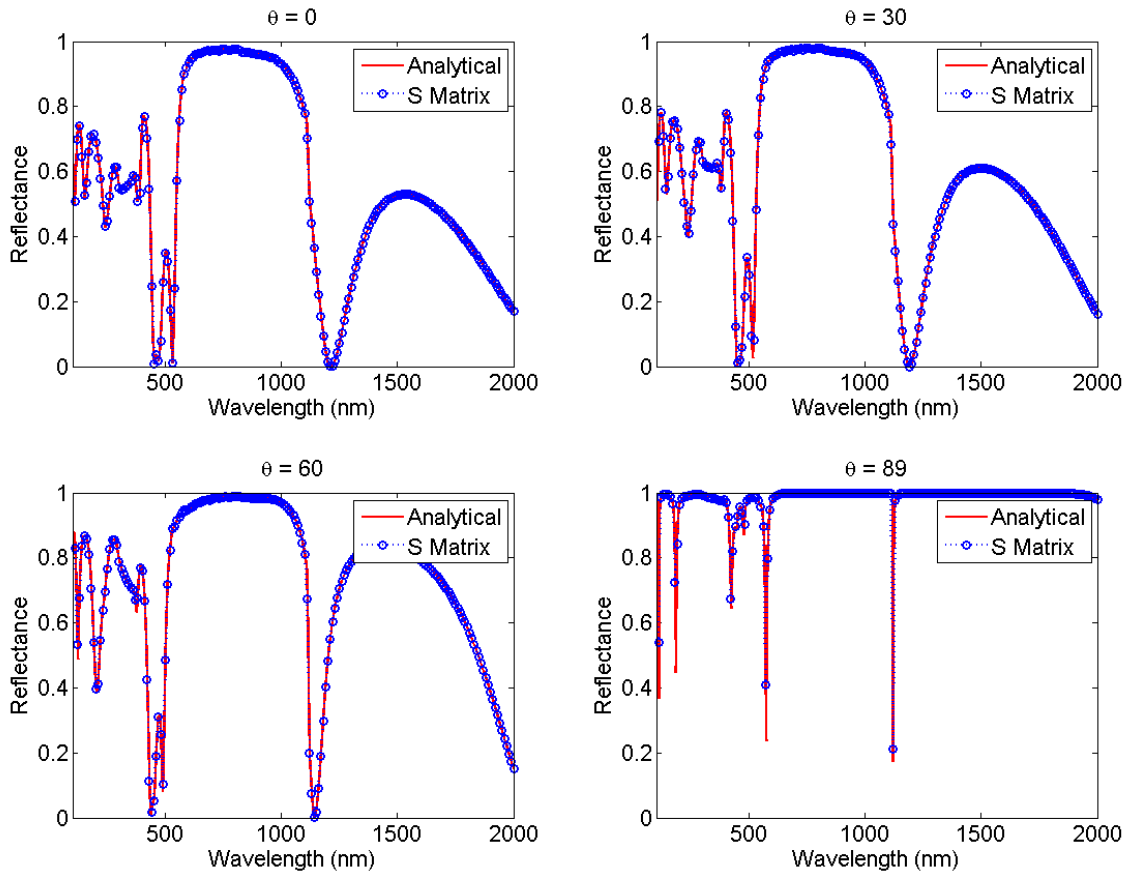


Figure 1.5 The reflectance from the 6-layer DBR for TE polarization at different angles, showing excellent agreement with scattering matrix simulations.

constant of ITO is 1.95, so the contrast ratio of the two materials is smaller than the previous design. As a result, the bandgap is smaller and more layers of the materials are needed to provide high reflectivity. In the case of  $\text{SiO}_2$  and silicon DBR, 6 layers can provide reflectance of  $\sim 97\%$  inside the bandgap (Fig. 1.7a). For ITO and silicon DBR, at least 10 layers are required to provide same level of reflectance (Fig. 1.7b). Also the width of the bandgap is much smaller.

## 2D Photonic Crystal Slab

We now survey basic properties of two-dimensional photonic crystals. Photonic crystal slabs are important class of photonic crystal structures. Due to their ease of fabrication,

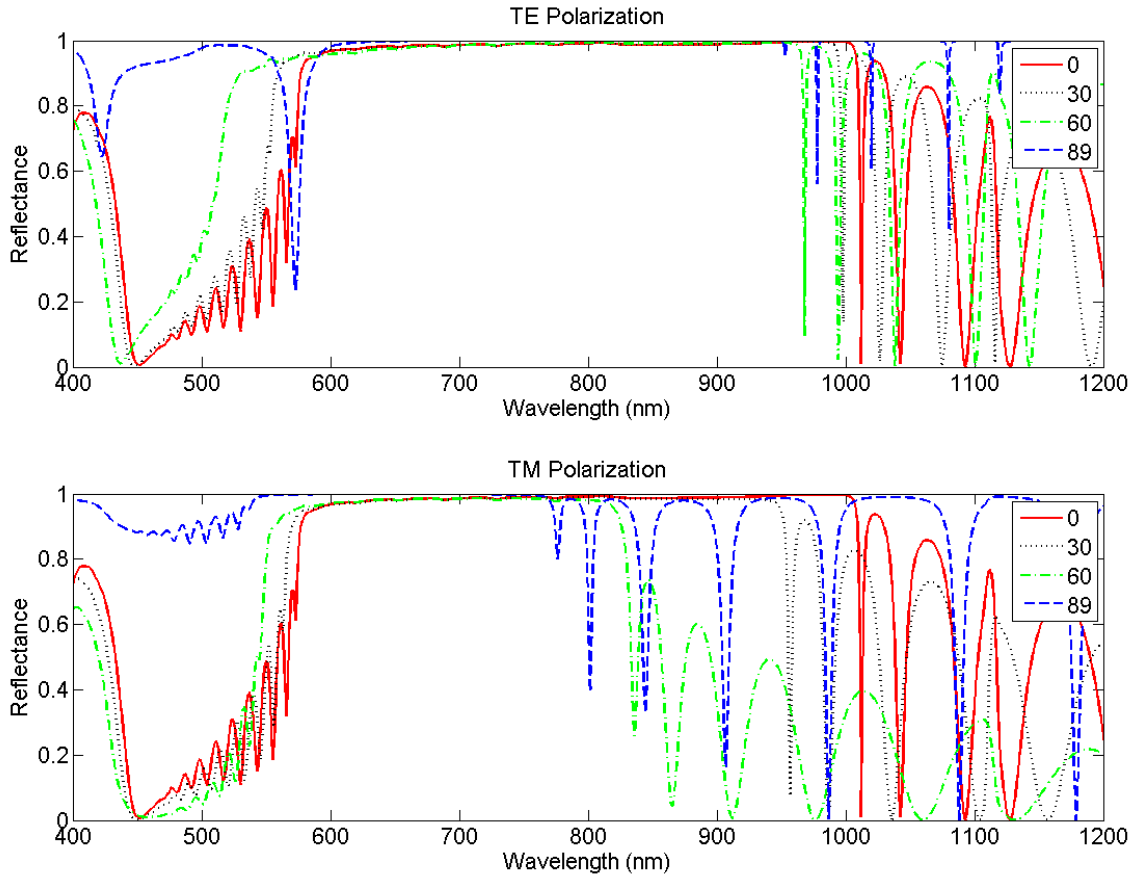


Figure 1.6 The angular dependency of the reflectance from the 30-layer DBR for both polarizations. The photonic bandgaps change with incident angles.

photonic crystal slabs have attracted lots of attention. A photonic crystal slab consists of two dimensional periodic variations in dielectric indices. Figure 1.8 shows photonic crystal slab structures with square lattice and triangular lattice of cylinders in high dielectric index a-Si:H slabs. The filling material of the cylinders can be either  $\text{SiO}_2$  or ITO.

The 2D photonic crystal slab can act as diffraction grating used in the solar cells. The incident and reflected field components are depicted in figure 1.9. The wave vector and electric field vector of the incident field can be defined as,

$$\mathbf{k}_i = k_{ix}\hat{\mathbf{x}} + k_{iy}\hat{\mathbf{y}} + k_{iz}\hat{\mathbf{z}} \quad (1.14)$$

$$\mathbf{E}_i = \mathbf{E}_0 \exp(-j\mathbf{k}_i \cdot \mathbf{r}) = \mathbf{E}_0 \exp[-j(k_x x + k_y y + k_z z)] \quad (1.15)$$

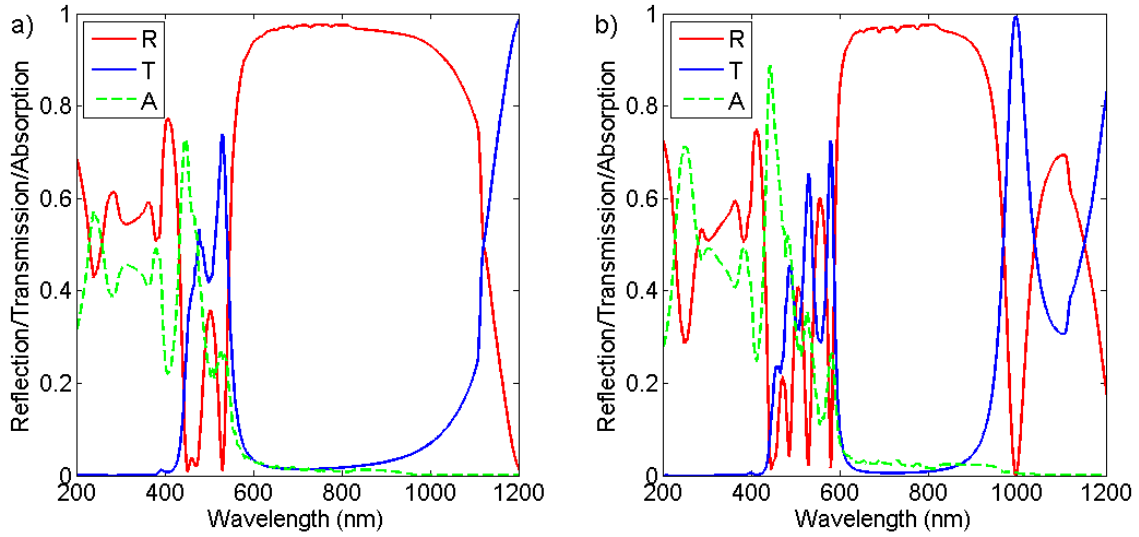


Figure 1.7 a) The reflection, transmission and absorption of 6-layer SiO<sub>2</sub>/Si DBR at normal incidence. b) The reflection, transmission and absorption of 10-layer ITO/Si DBR at normal incidence.

The reflected field vector can then be expressed in terms of Rayleigh expansions [8, 9],

$$\mathbf{E}_r = \sum_{m,n} \mathbf{R}_{mn} \exp(-j\mathbf{k}_{r,mn} \cdot \mathbf{r}) \quad (1.16)$$

The integer  $m$  and  $n$  define the order of the diffracted waves.  $\mathbf{R}_{mn}$  is the magnitude of the ( $m$ ,  $n$ ) diffracted wave.

From the phase matching condition and Floquet condition,

$$\mathbf{k}_{r,mn} = k_{xm}\hat{\mathbf{x}} + k_{yn}\hat{\mathbf{y}} + k_{zr,mn}\hat{\mathbf{z}} \quad (1.17)$$

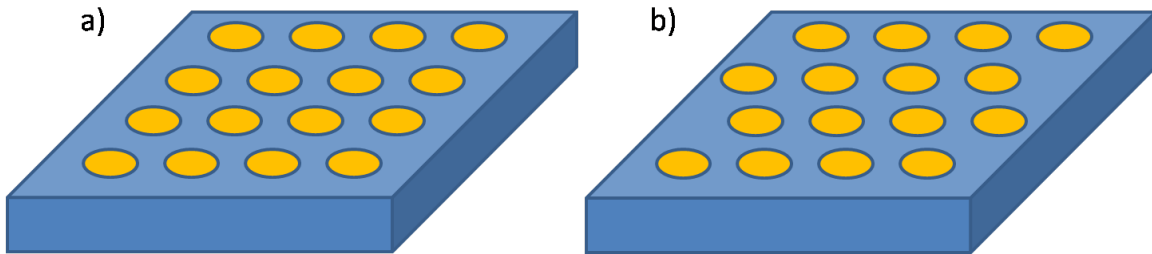


Figure 1.8 a) 2D photonic crystal structure with square lattice of cylinders in a dielectric slab. b) 2D photonic crystal structure with square lattice of cylinders in a dielectric slab.

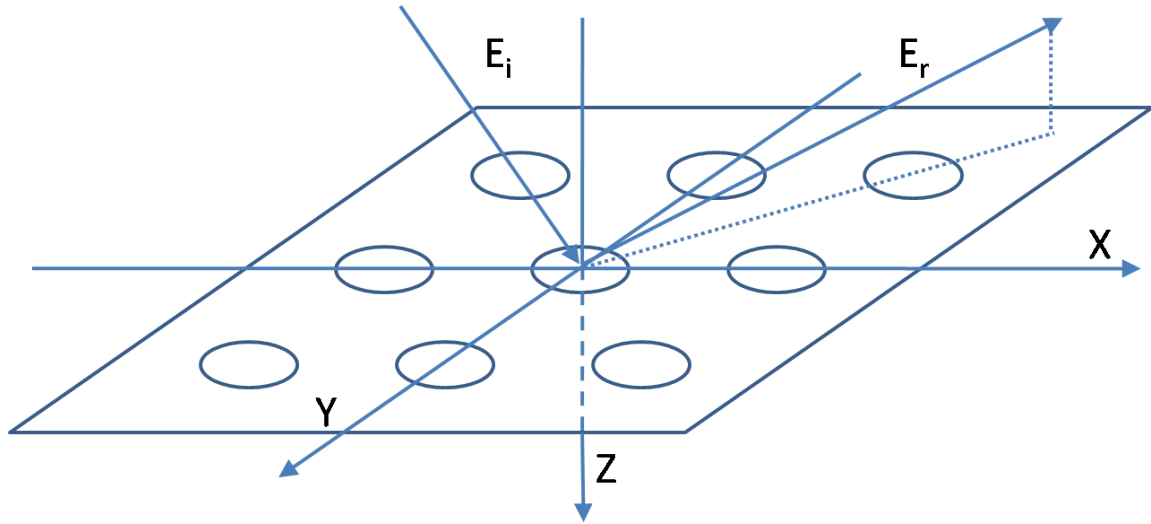


Figure 1.9 The schematics of the incident wave and reflected wave from the 2D square lattice photonic crystal slab.

where,

$$\begin{aligned}
 k_{xm} &= k_x + mG_x \\
 k_{yn} &= k_y + nG_y \\
 k_{zr,mn}^2 &= k_i^2 - k_{xm}^2 - k_{yn}^2
 \end{aligned} \tag{1.18}$$

$G_x$  and  $G_y$  are unit vectors of the reciprocal lattice vector  $G$ . They are also referred to as grating vectors in diffraction gratings. In square lattice showed in figure 1.9,

$$G_x = G_y = 2\pi/a \tag{1.19}$$

where  $a$  is the lattice constant. If  $k_{zr,mn}^2 > 0$ , the reflected wave is a propagating wave; otherwise, it is an evanescent wave which decays exponentially away from the interface.

### Scattering Matrix Method

The principal simulation method employed in the thesis is the Scattering Matrix Method. We briefly survey the method since extensive discussions appear in published papers. The well-known Transfer Matrix Method (TMM) can be used to calculate the transmission and reflection

spectra from layer by layer structures [10, 11]. In each layer, the material is homogeneous along the z direction (Fig 1.10).  $\Omega$ s are column vectors consisted of Fourier components of electric fields. A transfer matrix can be defined relating the incident, transmitted and reflected fields for each layer,

$$\begin{pmatrix} \Omega_i^+ \\ \Omega_i^- \end{pmatrix} = T_i \begin{pmatrix} \Omega_{i-1}^+ \\ \Omega_{i-1}^- \end{pmatrix} \quad (1.20)$$

Then the total transfer matrix can be obtained by multiplication of transfer matrices for all the layers.

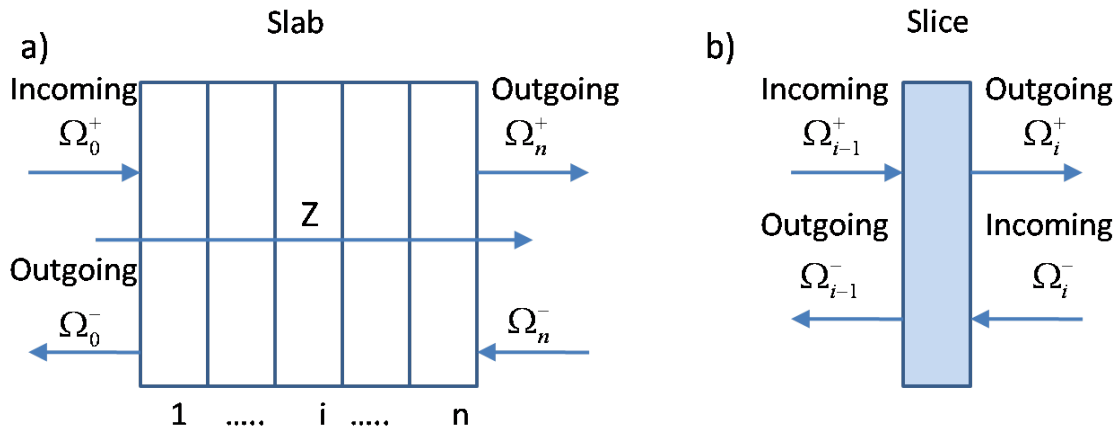


Figure 1.10 Definition of S matrix for photonic crystal slab with n layers.  
b) Definition of S matrix for an individual layer.

But for large layer thickness, TMM has been proved to be numerically unstable. The stability issue can be solved by redefine the transfer matrix as scattering matrix (S matrix),

$$\begin{pmatrix} \Omega_i^+ \\ \Omega_{i-1}^- \end{pmatrix} = s^i \begin{pmatrix} \Omega_{i-1}^+ \\ \Omega_i^- \end{pmatrix} \quad (1.21)$$

Then a recursion algorithm is used to connect each individual S matrix to the total S matrix [12].

The S matrix for each layer can be calculated from the continuity of  $\mathbf{E}$  and  $\mathbf{H}$  fields on each interface. In each layer, the dielectric index  $\epsilon$  is a function of x and y only. The Fourier

transforms of  $\epsilon$  and  $\epsilon^{-1}$  can be expressed as,

$$\epsilon(\mathbf{r}) = \sum_{ij} \epsilon_{ij} \exp(-j\mathbf{G}_{ij} \cdot \mathbf{r}) \quad (1.22)$$

$$\epsilon^{-1}(\mathbf{r}) = \sum_{ij} \epsilon_{ij}^{-1} \exp(-j\mathbf{G}_{ij} \cdot \mathbf{r}) \quad (1.23)$$

where  $\mathbf{r} = x\hat{\mathbf{x}} + y\hat{\mathbf{y}}$ . The Maxwell's equations 1.5 can be decomposed into 6 equations in three dimensional Cartesian coordinate system. The z dependence of the in-plane electric fields can be obtained,

$$\frac{\partial}{\partial z} E_x = \frac{1}{jk_0} \frac{\partial}{\partial x} \left[ \frac{1}{\epsilon(x,y)} \left( \frac{\partial}{\partial x} H_y - \frac{\partial}{\partial y} H_x \right) \right] - jk_0 H_y \quad (1.24)$$

$$\frac{\partial}{\partial z} E_y = \frac{1}{jk_0} \frac{\partial}{\partial y} \left[ \frac{1}{\epsilon(x,y)} \left( \frac{\partial}{\partial y} H_x - \frac{\partial}{\partial x} H_y \right) \right] + jk_0 H_x \quad (1.25)$$

Each field is rewritten in the forms of equation 1.16. Substituting 1.23 into 1.24 and 1.25,

$$\frac{\partial}{\partial z} E_{ij,x} = \frac{jk_{ij,x}}{k_0} \sum_{mn} \epsilon^{-1}{}_{ij,mn} (k_{mn,x} H_{mn,y} - k_{mn,y} H_{mn,x}) - jk_0 H_{ij,y} \quad (1.26)$$

$$\frac{\partial}{\partial z} E_{ij,y} = \frac{jk_{ij,y}}{k_0} \sum_{mn} \epsilon^{-1}{}_{ij,mn} (k_{mn,x} H_{mn,y} - k_{mn,y} H_{mn,x}) + jk_0 H_{ij,x} \quad (1.27)$$

Two more equations for the magnetic field can be derived following the same procedure. With the column vectors  $E = (\dots, E_{ij,x}, E_{ij,y}, \dots)^T$  and  $H = (\dots, H_{ij,x}, H_{ij,y}, \dots)^T$ , equations 1.26 and 1.27 can be written in matrix form,

$$\frac{\partial}{\partial z} E = T_1 H \quad (1.28)$$

And similarly,

$$\frac{\partial}{\partial z} H = T_2 E \quad (1.29)$$

Finally,

$$\frac{\partial^2}{\partial z^2} E = T_1 T_2 E = PE \quad (1.30)$$

The eigenvalue equation 1.30 is then solved for each layer with boundary conditions that the fields are continuous at the interfaces. The solutions will lead to S matrix for each layer.



Standard recursion relations are then used to construct the scattering matrix of the entire structure  $S$  from the scattering matrices ( $S^i$ ) of the individual layers. From the scattering matrix  $S$  the reflection, transmission and absorption of any layered structure can be simulated when waves are incident from the left or from the right of the structure.

There are several advantages of the scattering matrix method over traditional methods such as finite difference time domain (FDTD). In the scattering matrix method Maxwell's equations are solved in Fourier space for each frequency at a time i.e. in the frequency domain. There is no need to use a real space grid which is a major drawback in dealing with thick substrates or thick layers. The use of real space grids in FDTD demand enormous use of memory. The Fourier space approach has the advantage that any number of layers of differing width can be easily described since a real-space grid is not needed.

Since the scattering matrix is being employed in frequency domain, the computational algorithm can be easily parallelized with each frequency of group of frequencies sent to a different processor. Such a parallelization is difficult to achieve with real-space methods. The results for each frequency are then concatenated to obtain the entire frequency response of the system.

The convergence of scattering matrix method is fast for dielectric materials compared with metallic materials, since dielectrics do not have dispersion as strong as metals. A plane wave number of 261 is sufficient for modeling our solar cell structures. On the cluster mountain (mountain.ece.iastate.edu), it takes  $\sim 10$  minutes to calculate the transmission and reflection for each frequency on one processor. On the cluster cyblue (cyblue.ece.iastate.edu), it takes  $\sim 30$  minutes to complete the calculation. Thanks to large number of processors available on cyblue, up to 512 processors can be allocated at once and the total absorption can be obtained for the whole solar spectrum in a single run.

## Thesis Organization

Chapter 2 and 3 are two papers published Material Research Society Symposium Proceeding and Journal of Applied Physics. They describe the enhanced light-trapping in a-Si:H solar

cells with 2D photonic crystal grating and DBR. Chapter 2 uses SiO<sub>2</sub> and silicon to form the grating and the DBR, while chapter 3 uses ITO and silicon.

In chapter 4, periodic array of gold nano-cylinders are formed on top the ITO substrate. Incoming light can be diffracted from the normal direction with little loss. The concept can be applied to solar cell structure and light-trapping enhancement is expected. This chapter serves as suggestions for future work.

## References

1. J. Nelson, *The Physics of Solar Cells* (Imperial College Press, London, 2003)
2. E. Yablonovitch, *J. Opt. Soc. Am.* **72**, 899 (1982)
3. Springer, A. Poruba, L. Mullerova, M. Vanecek, O. Kluth and B. Rech, *J. Appl. Phys.* **95**, 1427 (2004).
4. B. Yan, J. M. Owens, C. Jiang, J. Yang and S. Guha, *Mater. Res. Soc. Symp. Proc.* **862**, 603 (2005).
5. J. D. Joannopoulos, R. D. Meade and J. N. Winn, *Photonic Crystals* (Princeton University Press, Princeton, NY, 1995).
6. Y. Fink, J. N. Winn, S. Fan, C. Chen, J. Michel, J. D. Joannopoulos and E. L. Thomas, *Science.* **282**, 1679 (1998).
7. P. Yeh, *Optical Waves in Layered Media* (John Wiley & Sons, Hoboken, New Jersey, 2005).
8. R. Petit, *Electromagnetic Theory of Gratings* (Springer-Verlag, Berlin, 1980).
9. S. Peng and G. M. Morris, *J. Opt. Soc. Am. A.* **13**, 993 (1996).
10. Z. Y. Li and L. L. Lin, *Phys. Rev. E* **67**, 046607 (2003).
11. R. Biswas, C.G. Ding, I. Puscasu, M. Pralle, M. McNeal, J. Daly, A. Greenwald and E. Johnson, *Phys. Rev. B* **74**, 045107 (2006).
12. L. Li, *J. Opt. Soc. Am. A.* **13**, 1024 (1996).

## CHAPTER 2 ENHANCING AND EFFICIENCY OF SOLAR CELLS WITH PHOTONIC CRYSTALS

A paper published in Mater. Res. Soc. Symp. Proc. **989**, A03.02 (2007)

Rana Biswas<sup>1</sup> and Dayu Zhou<sup>2</sup>

<sup>1</sup>Departments of Physics and Astronomy, Electrical and Computer Engineering, Microelectronics Research Center and Ames Laboratory, Iowa State University, Ames, Iowa 50011

<sup>2</sup>Department of Electrical and Computer Engineering and Microelectronics Research Center, Iowa State University, Ames, Iowa 50011

### Abstract

A major route to improving solar cell efficiencies is by improving light trapping in solar cell absorber layers. Traditional light trapping schemes involve a textured metallic back reflector that also introduces losses at optical wavelengths. Here we develop alternative light trapping schemes for a-Si:H thin film solar cells, that do not use metallic components, thereby avoiding losses. We utilize low loss one dimensional photonic crystals as distributed Bragg reflectors (DBR) at the backside of the solar cells. The DBR is constructed with alternating layers of crystalline silicon and SiO<sub>2</sub>. Between the DBR and the absorber layer, there is a layer of two dimensional photonic crystal composed of amorphous silicon and SiO<sub>2</sub>. The 2D photonic crystal layer will diffract light at oblique angles, so that total internal reflections are formed inside the absorber layer. We have achieved very high optical absorption throughout optical wavelengths (400 – 700 nm) and enhanced light-trapping at near-infrared (IR) wavelengths (700 – 800 nm) for amorphous silicon solar cell. The optical modeling is performed with a

rigorous three dimensional scattering matrix approach where Maxwell's equations are solved in Fourier space.

## Introduction

Enhancing light-trapping is a major route to improving solar cell efficiency. Typically, enhancing light-trapping in thin film solar cells is achieved by a back reflector that confines light within the absorber layer. The back reflector is usually textured to scatter light at the interface through large reflected angles. This increases the optical path length within the cell i-layer, and it is necessary to scatter as much light as possible in oblique directions.

A typical metallic back reflector consisting of Ag coated with ZnO [1], suffers from intrinsic losses. The granularity of the interface [1] produces small metallic nanoparticles that can exhibit surface plasmon modes. Surface plasmons of free Ag nano-particles are at ultraviolet wavelengths. Ag coated with a dielectric (with refractive index  $n$ ), has surface plasmon wavelengths lowered by  $\sim 1/n$ , and can reside at optical wavelengths. Such surface plasmon modes induce intrinsic loss with every light passage in the cell, which was measured by Springer et al [2] to be 3% to 8% at 650 nm for different surface roughness of the silver back reflector. The losses accumulate and become severe at infrared wavelengths where the absorption length of photons in a-Si:H is long and multiple optical passes are required. Even a small loss of 4% with each reflection in a metallic back-plane incurs a severe loss of  $1 - (0.96)^{50}$  or 87% with 50 passes. These considerations have motivated us to examine the novel use of loss-less nonmetallic photonic crystal structures for light-trapping.

## Background

Photonic crystals (PCs) have been a major scientific revolution in manipulating and guiding light in novel ways [3]. It is likely that photonic crystals can be utilized to harvest solar photons in ways not possible conventionally. Heine and Dorf [4] utilized gratings to enhance absorption in solar cells. Two groups at MIT [5,6] have recently developed a novel scheme for enhancing light-trapping in c-Si solar cells, where the metallic back-reflector was replaced by a DBR with

a reflective band at near-IR wavelengths ( $\lambda > 0.8 \mu m$ ) where the absorption lengths of photons are large. A diffractive grid on the DBR reflected light at oblique angles to increase the path lengths of near IR photons.

In the limit of a loss-less random metallic scattering surface, geometrical optics predicts an increase of optical path length by at most  $4n^2$  [7] corresponding to  $\sim 45$  for Si ( $n$  is the refractive index of the absorber). However, in conventional light-trapping schemes considerably less path length enhancement ( $\sim 10$ ) can be achieved. The advantage of photonic crystals is to introduce diffraction, where the photon momentum ( $\mathbf{k}$ ) can be scattered away from the specular direction with ( $\mathbf{k}^{\parallel} = \mathbf{k}_i^{\parallel} + \mathbf{G}$ ), where  $\mathbf{G}$  is a reciprocal lattice vector. As emphasized in recent work by MIT groups [5, 6], diffractive wave optics can enhance the path length of light far in excess of the classical limit of  $4n^2$  from geometrical optics.

## Theoretical Model

We simulate solar cell structures with a rigorous scattering matrix method [8], where Maxwell's equations are solved in Fourier space and the electric/magnetic fields are expanded in Bloch waves. The structure is divided into slices (along  $z$ ). In each slice the dielectric function  $\epsilon(r)$  is a periodic function of  $x$  and  $y$ . Hence the dielectric function and its inverse are Fourier expansions with coefficients  $\epsilon(G)$  and  $\epsilon^{-1}(G)$ .

In the scattering matrix method [8, 9], a transfer matrix  $M$  in each layer is calculated and diagonalized to obtain the eigenmodes within each layer. Both polarizations are included. The continuity of the parallel components of  $\mathbf{E}$  and  $\mathbf{H}$  at each interface leads to the scattering matrices  $s_i$  of each layer, from which we obtain the scattering matrix  $S$  for the entire structure. Using the  $S$ -matrix, we simulate the reflection, transmission and absorption [9] for incident light. The advantage of this approach is that any number of layers of differing widths can be easily simulated since a real-space grid is not necessary. Since the solutions of Maxwell's equations are independent for each frequency, the computational algorithm has been parallelized where each frequency is simulated on a separate processor. The individual layers utilize realistic frequency dependent dielectric functions that include absorption and dispersion.

We focus on optical engineering of single junction cells, which ideally have a-Si:H absorbers with band gaps  $\sim 1.6$  eV. We use the frequency dependent dielectric functions  $(\epsilon_1, \epsilon_2)$  (Fig. 2) determined from spectroscopic ellipsometry for a-Si:H and analytically continued to the infrared by Ferlauto et al [10]. The absorption length  $\zeta(\lambda)$  of photons ( $\zeta = 1/\alpha = 1/4\pi n_2$ ) ;  $1 \mu m$  below wavelengths of  $0.65 \mu m$  (Fig. 2) and these photons can be absorbed effectively in thin ( $\sim 0.5 \mu m$ ) a-Si:H layer. However, when  $\lambda > 0.65 \mu m$ , the absorption length exceeds  $1 \mu m$  and in the near-IR below the band gap wavelength ( $0.7 - 0.775 \mu m$ ),  $\zeta$  exceeds  $5 \mu m$ . It is very difficult to harvest these near-IR photons. It is necessary to have lossless multiple reflections within the absorber, for effective light-trapping.

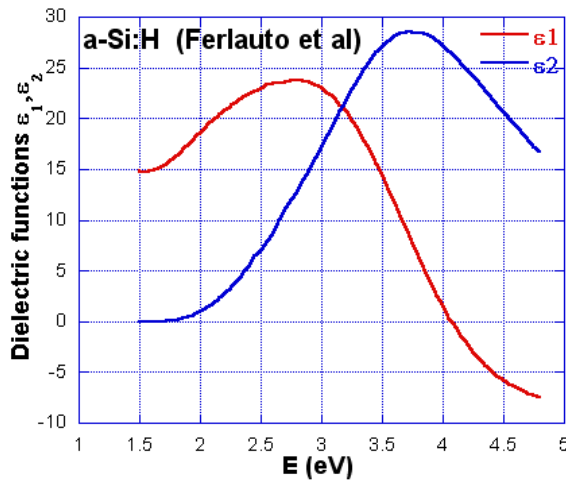


Figure 2.1 Energy dependent dielectric functions for a-Si:H with  $E_g = 1.6$  eV, determined from spectroscopic ellipsometry by Ferlauto et al (Ref [10]).

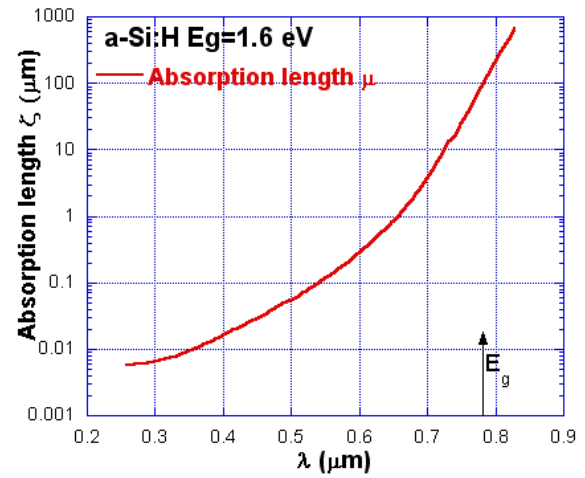


Figure 2.2 Absorption length of photons as a function of wavelength for a-Si:H with  $E_g = 1.6$  eV. The wavelength corresponding to the band edge  $E_g$  is indicated by the arrow.

## Light-trapping Schemes

The solar cell that we simulate (Fig2.3) consists of the following layers:

- i) The top indium tin oxide (ITO) layer ( $n = 1.95$ ), is an antireflective coating and top contact with a thickness ( $d_0$ ) that is determined using scattering matrix simulation.

ii) The a-Si:H absorber layer has a thickness of  $0.5 \mu\text{m}$ , typical for single-junction thin film solar cells. The bandgap is  $1.6 \text{ eV}$  ( $\lambda_g = 0.775 \mu\text{m}$ ).

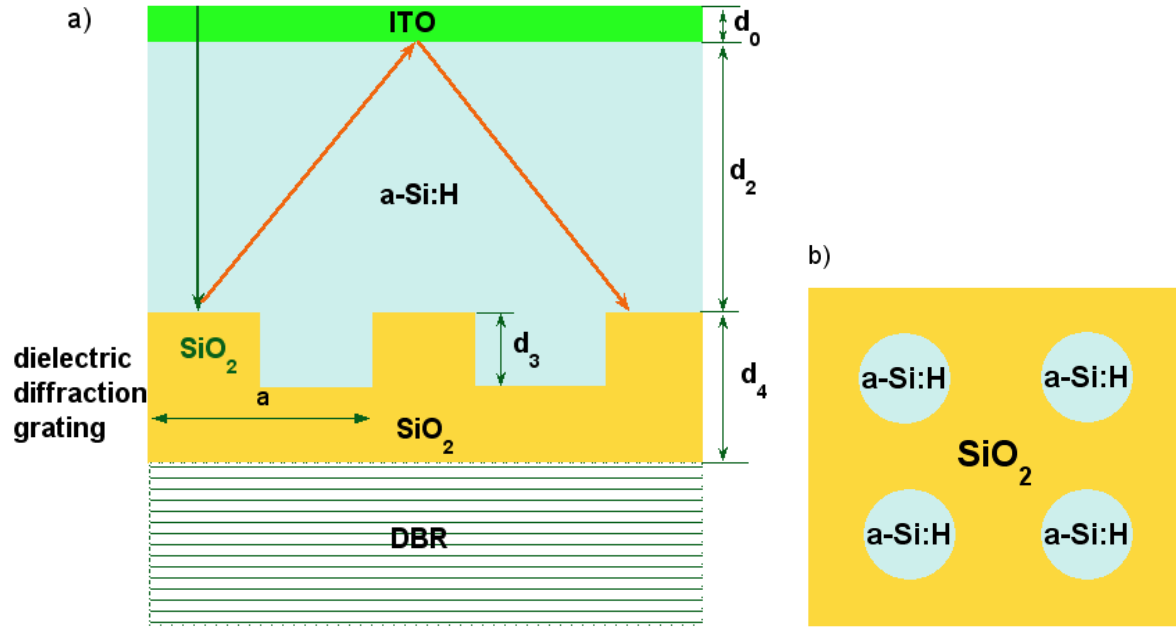


Figure 2.3 (a) Schematic solar cell configuration with antireflective coating, two-dimensional photonic crystal and distributed Bragg reflector (DBR) (b) Top view of 2D photonic crystal grating layer with amorphous silicon cylinders in SiO<sub>2</sub> background

iii) The two dimensional (2D) photonic crystal layer is a square lattice (lattice constant  $a$ ) of dielectric cylinders (radius  $R$ ) within another dielectric background material. The dielectric contrast of the two materials needs to be high enough for sufficient diffraction. We choose a-Si:H ( $n \approx 4$ ) and SiO<sub>2</sub> ( $n = 1.46$ ) as grating materials. There are two alternative designs, with a-Si:H cylinders in an SiO<sub>2</sub> background (Fig. 2.3b) or SiO<sub>2</sub> cylinders in an a-Si:H matrix. The PC layer thickness (grating depth  $d_3$ ) and lattice constant  $a$  are varied to maximize the absorption.

iv) The DBR of 6 alternating c-Si and SiO<sub>2</sub> layers represents an economical method for making an omni-directional reflector, that is much simpler than fabrication of 3D PCs. c-Si is chosen because it has a high index contrast ( $n \sim 3.8$ ) with SiO<sub>2</sub> ( $n = 1.46$ ) and low absorption. Although a-Si:H has a high refractive index, it also has considerable absorption, which is not desirable for the DBR. With c-Si thickness  $d_1 = 50 \text{ nm}$  and SiO<sub>2</sub> thickness  $d_5 = 120 \text{ nm}$ , an omni-directional bandgap from 565 to 788 nm is obtained [11]. The incident light in the absorber layer is confined in a small light cone ( $\alpha < 16^\circ$ ). The closer the incident light is to the normal, the wider the bandgap (Fig. 2.4).

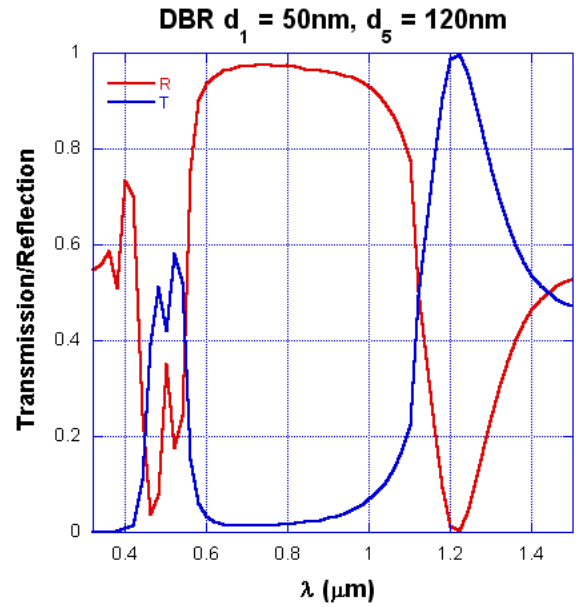


Figure 2.4 Reflection and transmission through 6-layer c-Si/SiO<sub>2</sub> DBR for normal incidence

## Simulation and Results

We understand the functions of different components of the solar cell separately. As shown above, the DBR provides a wide reflective stop band. To understand the diffraction of the 2D PC within the absorber layer, we simulate just the grating consisting of SiO<sub>2</sub> cylinders in an a-Si background in air on a thick ( $\sim 300 \mu\text{m}$ ) c-Si substrate. We obtain reflectance for different  $R/a$  with fixed grating depth ( $d_3 = 40 \text{ nm}$ ) and lattice constant ( $a = 0.7 \mu\text{m}$ ). By comparing the difference between specular and non-specular reflection, we can examine the effectiveness of the diffraction grating (Fig. 2.5). Diffraction occurs when  $\lambda < a$ . The maximum diffraction occurs between  $R/a = 0.35$  and  $0.4$ , when  $\sim 30\%$  of the light is diffracted. The value of  $R/a = 0.38$  also maximizes the strength of the Fourier component of grating.

Scattering matrix simulations are performed for the solar cell configuration of Fig. 2.3a and the absorption is maximized by varying one parameter at a time. An optimal structure consists



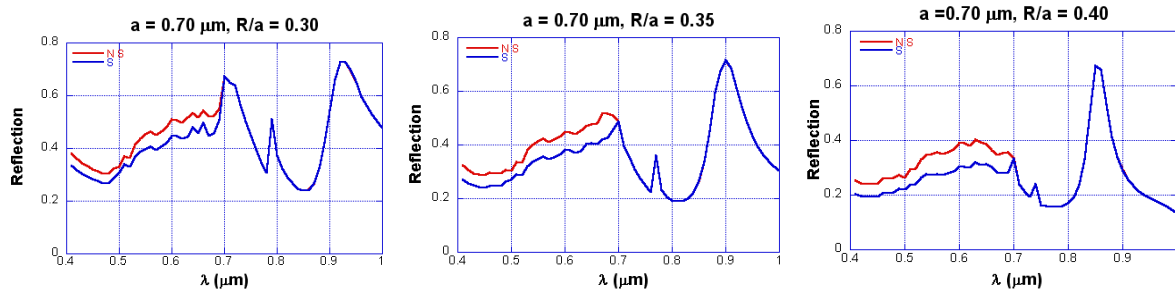


Figure 2.5 Comparison of specular (S) and non-specular (NS) reflection from the 2D photonic crystal for different  $R/a$  with  $a = 0.70 \mu m$ ,  $d_3 = 0.04 \mu m$  and  $d_4 = 300 \mu m$

of  $a = 600 \text{ nm}$ ,  $R/a = 0.38$ ,  $d_1 = 50 \text{ nm}$ ,  $d_2 = 500 \text{ nm}$ ,  $d_3 = 50 \text{ nm}$  and  $d_5 = 120 \text{ nm}$ . The thickness of ITO  $d_0$  is expected to range from  $500 \text{ nm}/4n_{ITO} = 64 \text{ nm}$  to  $775 \text{ nm}/4n_{ITO} = 100 \text{ nm}$ . By simulations, we find that  $d_0 = 65 \text{ nm}$  provides the least reflection from the top surface.

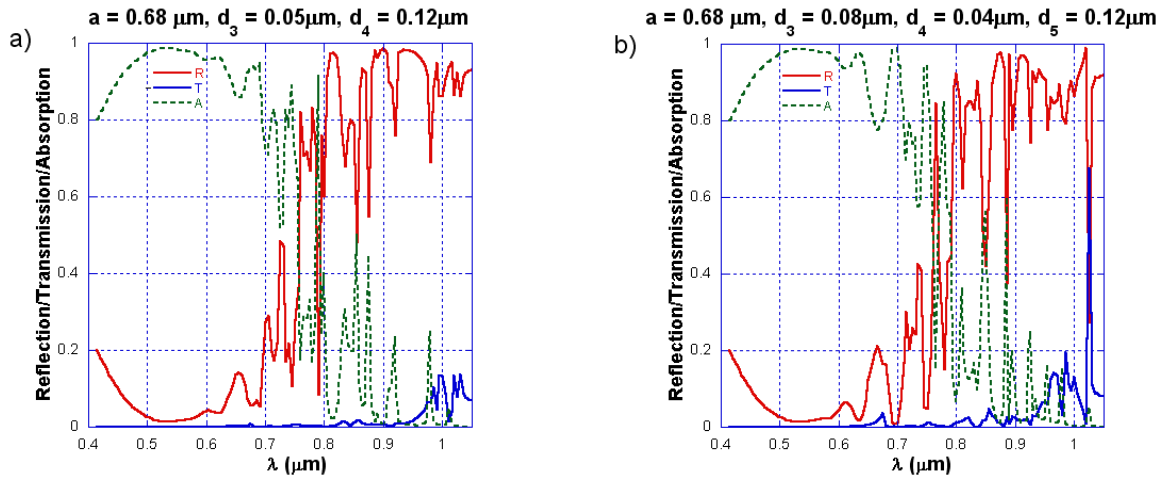


Figure 2.6 Non-specular (total) reflection/transmission/absorption in the absorber layers for the two competing designs with  $d_0 = 65 \text{ nm}$ ,  $d_1 = 50 \text{ nm}$ ,  $d_2 = 500 \text{ nm}$  and  $d_2 = 120 \text{ nm}$  (a) a-Si layer with  $\text{SiO}_2$  cylinders (b)  $\text{SiO}_2$  layer with a-Si cylinders

For fixed  $d_0 = 65 \text{ nm}$ , we optimize the lattice constant. We find that the lattice constants in the range from  $600$  to  $700 \text{ nm}$  give the highest absorption in the absorber layer, which correspond to the third order of diffraction. With  $a = 680 \text{ nm}$ , we run simulations with

different  $d_3$  for both grating configurations. We find that  $d_3 = 80 \text{ nm}$  for  $\text{SiO}_2$  layer with a-Si cylinders and  $d_3 = 50 \text{ nm}$  for a-Si layer with  $\text{SiO}_2$  cylinders give the best diffraction and highest light-trapping within the absorber layers.

The optimized solar cell with  $\text{SiO}_2$  cylinders inside the a-Si layer (Fig. 2.6a) and the complementary structure of a-Si cylinders in the  $\text{SiO}_2$  matrix (Fig. 2.6b) both show very high absorption ( $A > 0.8$ ) through most of the optical wavelengths ( $0.4 - 0.7 \mu\text{m}$ ) (Fig. 2.6) accompanied by small reflection. There is appreciable photon absorption between  $0.7 - 0.775 \mu\text{m}$ , a region where the absorption length of photons exceeds  $5 \mu\text{m}$ . The enhance absorption improves the near-IR solar response. Wavelengths larger than  $0.775 \mu\text{m}$  are largely reflected from the cell in both configurations and these are above the bandgap and do not contribute to photocurrent.

It is instructive to compare the light-trapping in our optimized solar cell with that of a bare a-Si:H film, an a-Si:H film with anti-reflective coating and an a-Si:H film with DBR and antireflective coating (Fig. 2.7). Below  $\lambda = 0.65 \mu\text{m}$ , the absorption length less than  $1 \mu\text{m}$ . With an anti-reflective coating and DBR, most of incident light can be absorbed in the absorber layer within two optical paths. Above  $\lambda = 0.65 \mu\text{m}$ , the PC enhances the light-trapping efficiency up to a factor of 2 without introducing losses.

The difference in grating depths of the two competing designs can be understood by different effective dielectric constants of the grating layers. With  $R/a = 0.38$ , the filling ratio  $f =$

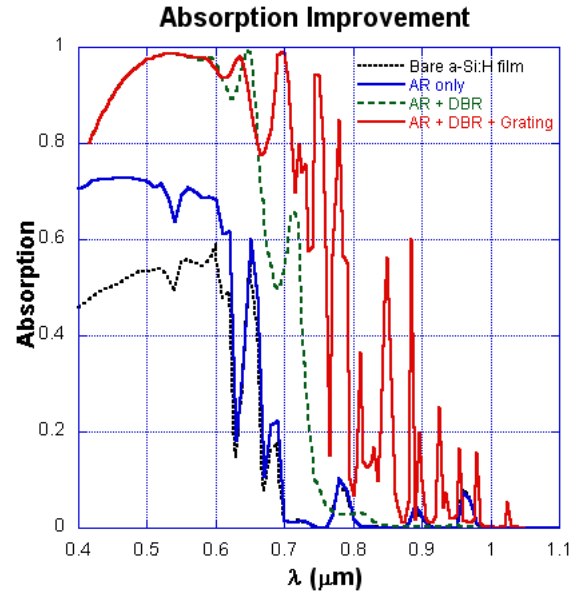


Figure 2.7 Comparison of absorption of a bare a-Si:H film, a-Si:H film with AR coating only, a-Si:H film with AR coating and DBR and the optimized solar cell with photonic crystal grating.

$\pi R^2/a^2 = 0.45$ . Maxwell-Garnett approximation gives  $n_{eff} \sim 3$  for a-Si grating layer and  $n_{eff} \sim 2.3$  for SiO<sub>2</sub> grating layer. Grating depth can be estimated by quarter wavelength inside the grating layer to reduce the specular reflection.

## Conclusions

We develop a novel light trapping scheme in a-Si:H solar cells with dielectric photonic crystals. By combining a 2D photonic crystal diffraction grating and DBR, we can efficiently harvest optical photons, without losses associated with metallic reflectors. We enhance the absorption at longer wavelength ( $\lambda > 0.65 \mu m$  – where absorption lengths are long) up to the bandgap by a factor of  $\sim 2$ . Also, the absorption peak of the optimized a-Si:H solar cell matches the peak of solar radiation spectrum. For future work, we wish to place a 2D photonic crystal diffraction grating at the interface between ITO and the absorber.

## Acknowledgements

We acknowledge support from the Catron Solar Foundation. The Ames Laboratory is operated for the Department of Energy by Iowa State University under contract No. W-7405-Eng-82. It is a pleasure to thank V. Dalal for many stimulating discussions and C.G. Ding for the initial scattering matrix computation code. We also acknowledge support from the NSF under grant ECS-06013177. We thank R. Collins and N. Podraza for kindly supplying the optical data for amorphous silicon films and the most helpful discussions.

## References

- [1] B. Yan, J. M. Owens, C. Jiang and S. Guha, MRS Symp. Proc. **862**, A23.3 (2005).
- [2] J. Springer, A. Poruba, L. Mullerova, M. Vanecek, O. Kluth and B. Rech, J. Appl. Phys. **95**, 1427 (2004).
- [3] J. D. Joannopoulos, R. D. Meade and J. N. Winn, *Photonic Crystals*, Princeton, NJ: Princeton University Press, 1995.
- [4] C. Heine, and R. H. Morf, Appl. Opt. **34**, 2476 (1995).

- [5] L. Zeng, Y. Yi, C. Hong, J. Liu, N. Feng, X. Duan, L.C. Kimmerling and B.A. Alamariu, Appl. Phys. Lett. **89**, 111111 (2006); MRS Symp. Proc. **862**, A12.3 (2005).
- [6] P. Bermel, C. Luo and J. D. Joannopoulos, to be published in Opt. Express (2007).
- [7] E. Yablonovitch and G. Cody, IEEE Transactions Electron Devices **ED-29**, 300 (1982).
- [8] Z. Y. Li and L. L. Lin, Phys. Rev. E **67**, 046607 (2003).
- [9] R. Biswas, C.G. Ding, I. Puscasu, M. Pralle, M. McNeal, J. Daly, A. Greenwald and E. Johnson, Phys. Rev. B. **74**, 045107 (2006).
- [10] A.S. Ferlauto, G. M. Ferreira, J. M. Pearce, C. R. Wronski, R. W. Collins, X. Deng and G. Ganguly, J. Appl. Phys. **92**, 2424 (2002).
- [11] Y. Fink, J. N. Winn, S. Fan, C. Chen, J. Michel, J. D. Joannopoulos and E. L. Thomas, Science. **282**, 1679 (1998).

## CHAPTER 3 PHOTONIC CRYSTAL ENHANCED LIGHT-TRAPPING IN THIN FILM SOLAR CELLS

A paper published in Journal of Applied Physics **103**, 093102 (2008)

Dayu Zhou<sup>1</sup> and Rana Biswas<sup>2</sup>

<sup>1</sup>Department of Electrical and Computer Engineering and Microelectronics Research Center, Iowa State University, Ames, Iowa 50011

<sup>2</sup>Departments of Physics and Astronomy, Electrical and Computer Engineering, Microelectronics Research Center and Ames Laboratory, Iowa State University, Ames, Iowa 50011

### Abstract

We utilize photonic crystals to simulate enhanced light-trapping in a-Si:H thin film solar cells. A one dimensional photonic crystal or distributed Bragg reflector with alternating dielectric layers acts as low loss backreflector. A two dimensional photonic crystal between the absorber layer and the Bragg reflector diffracts light at oblique angles within the absorber. The photonic crystal geometry is optimized to obtain maximum absorption. The photonic crystal provides lossless diffraction of photons, increasing the photon path length within the absorber layer. The simulation predicts significantly enhanced photon harvesting between 600 and 775 nm below the band edge, and an absorption increase by more than a factor of 10 near the band edge. The optical path length ratio can exceed the classical limit predicted for randomly roughened scattering surfaces at most wavelengths near the band edge. The optical modeling is performed with a rigorous scattering matrix approach where Maxwell's equations are solved in Fourier space.

## Introduction

Enhancing light-trapping is a major route to improving thin film solar cell efficiency. A major limitation to solar cell efficiency is the long absorption length of long wavelength photons and the small absorber layer thickness. Enhancing light-trapping in thin film solar cells is typically achieved by a textured metal back reflector that scatters light within the absorber layer and increases the optical path length of solar photons. A typical metallic back reflector of silver coated with ZnO (Ref. 1) suffers from intrinsic losses from surface plasmon modes generated at the granular metal-dielectric interface. Springer et al measured such losses to be 3% - 8% with each reflection at 650 nm, for different textured silver back reflectors.<sup>2</sup> Such losses accumulate rapidly and become even more severe at longer wavelengths, where the absorption lengths of photons in the absorber are increased and multiple optical passes are required.

Our analysis can be applied to any thin film solar cell, and we focus on a-Si:H as a convenient prototype. The absorption length ( $L_d$ ) of a-Si:H with bandgap ( $E_g$ ) of 1.6 eV is shown in Fig. 3.1, using measured dielectric functions.<sup>3</sup> For wavelengths  $\lambda > 650$  nm, the absorption length exceeds 1  $\mu$ m and approaches 100  $\mu$ m near the band edge ( $\lambda_g = 775$  nm, Fig. 3.1). It is exceedingly difficult to harvest these photons since the absorber thickness of p-i-n single junction solar cell is limited to a few hundred nm for efficient carrier collection. Improved harvesting of long wavelength photons is critical for enhancing the average absorptions and cell efficiencies.

Photonic crystals (PCs) have created a major scientific revolution in manipulating and guiding light in novel ways.<sup>4</sup> The advantage of photonic crystals is to introduce diffraction, where the photon momentum ( $\mathbf{k}$ ) can be scattered away from the specular direction with  $\mathbf{k}^{\parallel} = \mathbf{k}_i^{\parallel} + \mathbf{G}$ , where  $\mathbf{G}$  is a reciprocal lattice vector and  $\mathbf{k}_i$  is the incident wave-vector. Two groups have recently developed a novel scheme for enhancing light-trapping in crystalline silicon (c-Si) solar cells with a photonic crystal back reflector combined with a reflection grating.<sup>5,6</sup> This has motivated us to enhance light trapping in much thinner a-Si:H solar cells, using two-dimensional (2D) PCs as a diffraction grating.

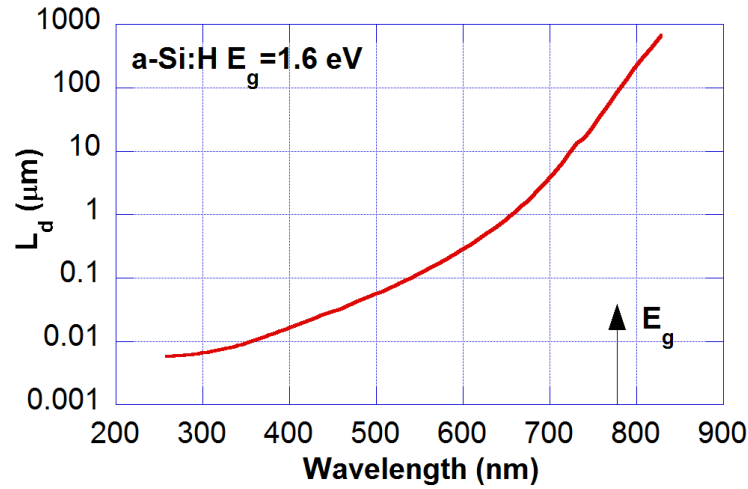


Figure 3.1 Absorption length of photons as a function of wavelength for a-Si:H with bandgap  $E_g = 1.6$  eV. The bandgap wavelength is indicated by the arrow.

### Light-trapping Schemes

We consider photonic crystal enhanced solar cells in which the metallic back-reflector is replaced by a distributed Bragg reflector (DBR) consisting of a one-dimensional dielectric superlattice [or one-dimensional (1D) photonic crystal] with sufficient dielectric contrast between the two components. In the photonic crystal enhanced solar configuration (Fig. 3.2), we have (1) a traditional antireflective coating as a top contact (thickness  $d_0$ ), (2) an absorber layer (thickness  $d_2$ ), (3) a two-dimensional photonic crystal (thickness  $d_3$ ) and (4) DBR. This configuration has the advantage that the diffraction of light occurs at the back of the cell where light absorption is very low. The 2D PC diffracts light within the absorber layer and the DBR specularly reflects light with little loss. Within the absorber layer, multiple total internal reflections occur and light is tightly trapped inside.

Various choices of DBR are possible. The DBR can be fabricated using  $n^+$  c-Si and ITO with thickness  $d_1 = 50$  nm and  $d_4 = 90$  nm. Although ITO offers low dielectric contrast ( $n_{ITO} \sim 1.95$ ), such a DBR is conductive and can be used directly as back contact — a significant advantage for solar cells. In contrast, another design utilizes 10 alternating layers

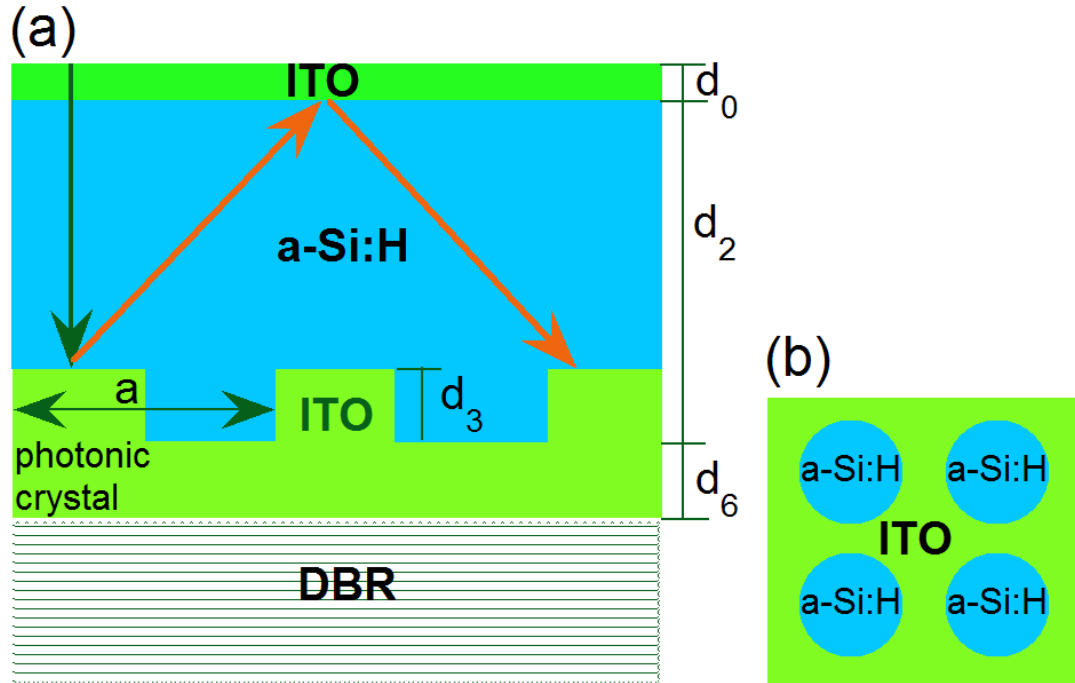


Figure 3.2 (a) Schematic solar cell configuration with top ITO, 2D PC, bottom ITO and DBR. (b) Top view of 2D PC grating layer with a-Si:H cylinders in an ITO background.

of c-Si and SiO<sub>2</sub> representing an economical method for making an insulating omni-directional reflector.<sup>7</sup> With a c-Si thickness  $d_1 = 50 \text{ nm}$  and a SiO<sub>2</sub> ( $n_{\text{SiO}_2} \sim 1.46$ ) thickness  $d_4 = 120 \text{ nm}$ , an omni-directional bandgap from 565 to 788 nm is obtained.<sup>8</sup> Within this range, nearly  $\sim 100\%$  of the incident photons are reflected. A thin ITO layer on top of the DBR, followed by interdigitated contacts to collect electrons on the side is necessary, which results in a complex device structure.

The PC is a square lattice (period of  $a$ ) of a-Si:H cylinders (radius of  $R$ ) enclosed by the oxide background. The dielectric contrast of the two materials ( $\sim 4$ ) is large enough for sufficient diffraction of light reflected from the PC. The absorber thickness ( $d_2$ ) is 500 nm, typical for single-junction or tandem cells. In order to account for p-layer losses in a p-i-n solar cell, we choose a p-layer thickness of  $d_p \sim 20 \text{ nm}$  that strongly absorbs at short wavelengths. The absorption  $A$  in the i-layer is  $A(\lambda) = A_t(\lambda) \exp(-d_p/L_d(\lambda))$ , where  $A_t(\lambda)$  is the total



absorption.

## Simulation and Results

We simulate solar cell structures with a rigorous scattering matrix method.<sup>9,10</sup> Maxwell's equations are solved for both polarizations in Fourier space and the electric/magnetic fields are expanded in Bloch waves. We use frequency dependent dielectric functions determined from spectroscopic ellipsometry that are analytically continued to the infrared by Ferlauto et al for a-Si:H.<sup>3</sup> Since Maxwell's equations for each frequency are independent, the computational algorithm has been parallelized where each frequency is simulated on a separate processor. The calculated total absorption in the i-layer is weighted by the AM 1.5 solar spectrum<sup>11</sup> and integrated from 280 nm ( $\lambda_{min}$ ) to 775 nm ( $\lambda_g$ ) to obtain the average absorption  $\langle A \rangle$

$$\langle A \rangle = \int_{\lambda_{min}}^{\lambda_g} A(\lambda) \frac{dI}{d\lambda} d\lambda \quad (3.1)$$

where  $dI/d\lambda$  is the incident solar radiation intensity per unit wavelength.

We systematically optimize each layer in the solar cell to achieve the highest light-trapping. It is convenient to start with a cell with the antireflective coating fixed to a value very close to a quarter-wavelength near the middle of the optical range ( $d_0 \sim 65$  nm at 500 nm).

The cylinder radius in the photonic crystal assumes a value that maximizes the diffraction from the photonic crystal. Maximum diffraction is expected when the Fourier components of the dielectric function of the 2D PC is a maximum. The Fourier component of an array of cylinders is known to be,<sup>9</sup>

$$\epsilon(G) = f(\epsilon_{Si} - \epsilon_{ITO}) \frac{2J_1(GR)}{GR} \quad (3.2)$$

where  $f = \pi R^2/a^2$  is the filling ratio. With  $R/a = 0.38$ , we maximize the strength (Fig. 3.3) of the first Fourier component ( $G_1 = 2\pi/a$ ). This radius is a useful guide for the initial simulations and will be later optimized carefully.

The thickness of the photonic crystal  $d_3$  is such that the specular reflected beam is minimized at the interface between a-Si:H and 2D photonic crystal grating. Inside the bandgap of DBR, the real part of effective impedance of the DBR ( $\eta_{23}$ ) is almost zero, so that the

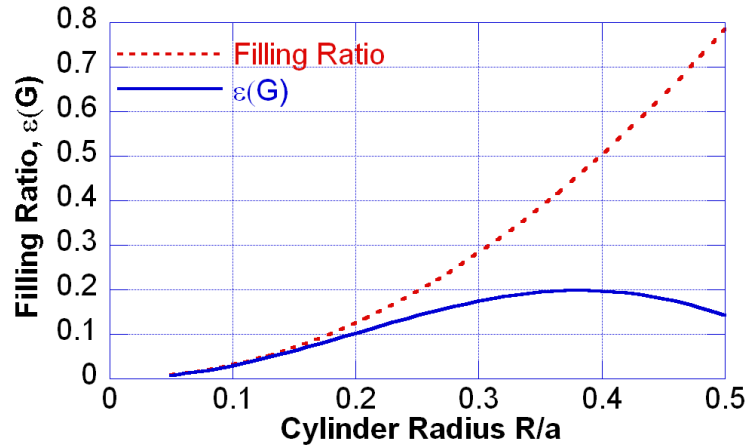


Figure 3.3 (Fourier component of the dielectric function and filling ratio, for the first reciprocal lattice vector  $G_1 = 2\pi/a$ .)

reflection coefficient ( $\Gamma_{23}$ ) at the surface of DBR has a magnitude of unity. Assuming normal incidence, the total reflection coefficient from the ITO portion of the photonic crystal grating is:

$$\Gamma_{ITO} = \frac{\Gamma_{12} + \Gamma_{23}e^{-j2\beta_{ITO}d_3}}{1 + \Gamma_{12}\Gamma_{23}e^{-j2\beta_{ITO}d_3}} \quad (3.3)$$

where  $\Gamma_{12} = (\eta_{ITO} - \eta_{a-Si})/(\eta_{ITO} + \eta_{a-Si})$  and  $\beta_{ITO}$  is the phase constant inside the ITO. The total reflection coefficient from the a-Si:H portion of the photonic crystal grating is:

$$\Gamma_{a-Si} = \Gamma_{23}e^{-j2\beta_{a-Si}d_3} \quad (3.4)$$

where  $\beta_{a-Si}$  is the phase constant inside a-Si:H.

The sum of the reflection coefficients from the ITO and a-Si:H portions should vanish for the choice of  $d_3$ . With this crude approximation, a 90 nm grating layer shows the minimum overall reflection. We can see later that the optimized value of 100 nm validates this approximation. Some initial simulations with these approximate parameters suggested that lattice constant of  $\sim 0.7 \mu\text{m}$  gave the best diffraction. We then optimized the PC thickness  $d_3$  and the ITO layer thickness  $d_6$  adjacent to the PC keeping other parameters constant. We found the best absorption for  $d_6 = 0$  and  $d_3 = 100 \text{ nm}$  (Fig. 3.4a) through scattering matrix simulations. However adding a thin base ITO layer for improving contacts will not reduce the absorption

very much (Fig. 3.4b). We therefore used the optimized value of  $d_3$  and  $d_6$  to optimize both the lattice spacing 'a' (Fig. 3.5) and the filling ratio of the photonic crystal or the cylinder radius R (Fig. 3.6).

The critical dependence of the enhanced absorption with the lattice spacing 'a' of the photonic crystal was obtained by calculating the absorption in the intrinsic layer (Fig. 3.5) with various choices of a, and holding other variables fixed. The average absorption (Fig. 3.5) is optimized for a lattice spacing  $a \sim 0.7 \mu m$ . However substantially larger lattice spacings near  $1 - 1.5 \mu m$  offer improvement over a flat metal reflector and may be much more convenient for fabrication. For diffraction from the PC, it is necessary for the lattice spacing of the photonic crystal be larger than the wavelength of light in the absorber layer ( $a > \lambda/n(\lambda)$ ). This condition is satisfied for  $a > 0.25 \mu m$ , where the enhanced absorption is found (Fig. 3.5).

The diffractive light-trapping mechanism can be explained by a simple analytical model. With the a-Si:H thickness  $d_2$ , all resonances should pick up a roundtrip phase change  $2m\pi$ , so that  $k_{\perp} = \pi m/d_2$ . The wavelength of diffracted resonant mode is given by:

$$\lambda = 2\pi n(\lambda) / \sqrt{G_x^2 + G_y^2 + (m\pi/d_2)^2} \quad (3.5)$$

where m is an integer, n is the refractive index of a-Si:H and  $G_x, G_y$  are the components of reciprocal lattice vectors ( $G_x = i(2\pi/a), G_y = j(2\pi/a)$ ). The diffraction resonances occur for integer values of i, j and m and exhibit peaks in the absorption for wavelengths near the band-edge for values of a larger than  $\sim 0.25 \mu m$ . The peaks overlap and form the overall absorption enhancement. It is necessary to have several diffraction resonances within the wavelength window ( $0.6 - 0.775 \mu m$ ) below the band edge, where the absorption length of photons is longer than the absorber layer thickness. Simulations indicate that the diffraction resonances are most effective for  $a \sim 0.7 \mu m$  (Fig. 3.5).

We varied the cylinder radius R/a, holding other parameters constant (Fig. 3.6) and found that the optimum value of cylinder radius occurs near  $R/a = 0.39 - 0.4$ , when the filling ratio is  $\sim 50\%$ . This value is as expected from the maximum magnitude of Fourier component of the dielectric function (Fig. 3.3) so that diffraction is most effective for near equal volume fraction of the two dielectric materials.

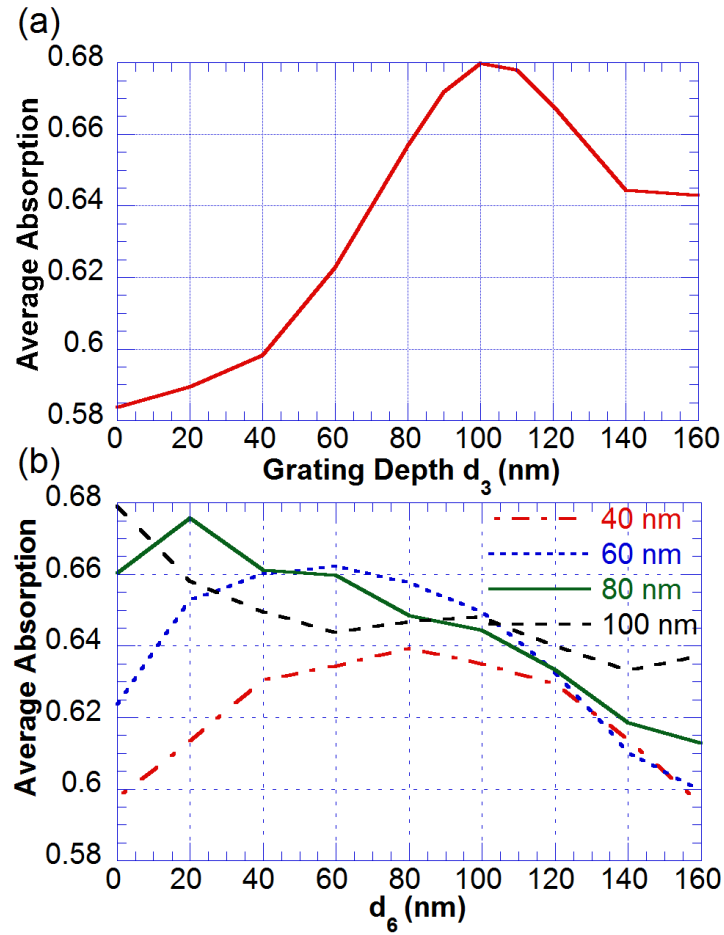


Figure 3.4 a) The variation in average absorption with thickness of the photonic crystal ( $d_3$ ), holding other parameters constant near the optimum values. b) The average absorption as a function of  $d_6$ , for several values of the grating depth  $d_3$ .

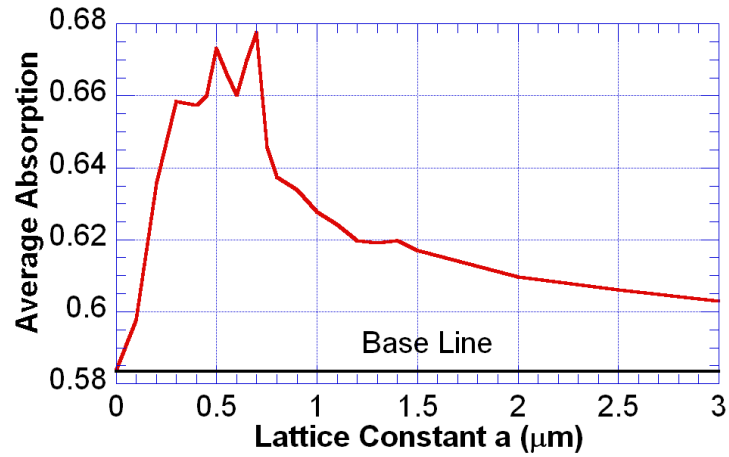


Figure 3.5 The variation in average absorption with lattice spacing 'a' of the photonic crystal, holding other parameters constant near the optimum values.

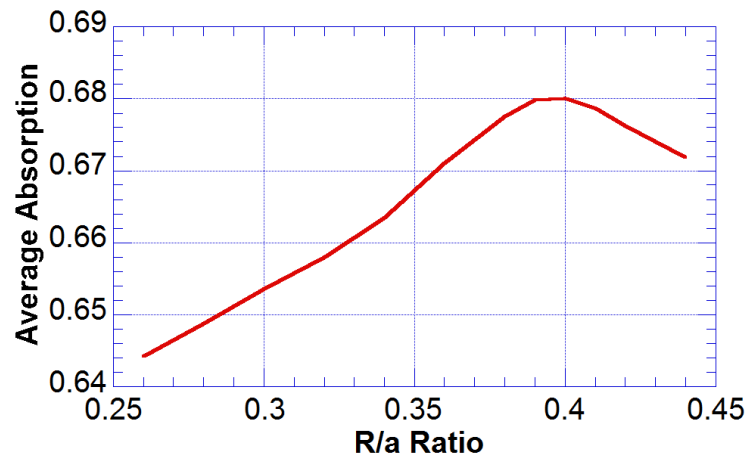


Figure 3.6 The variation in average absorption with cylinder radius of the photonic crystal, holding other parameters constant near the optimum values.

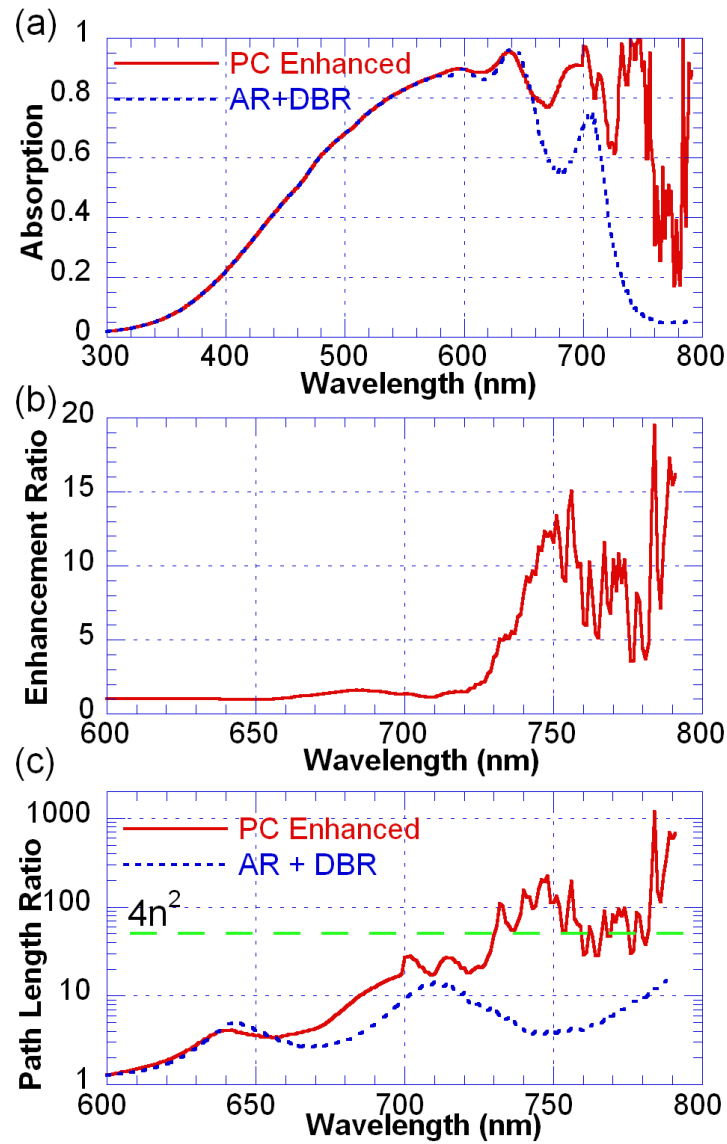


Figure 3.7 (a) The absorption of the optimized photonic crystal enhanced solar cell structure as a function of the wavelength, compared to the reference cell with antireflective coating and DBR only. (b) The absorption enhancement ratio of the optimized solar cell over the reference cell without the photonic crystal. (c) The ratio of the optical path length to the absorber layer thickness, for the optimized PC enhanced solar cell (solid) compared to the reference cell (dotted). The horizontal dashed line shows the theoretical limit of path length enhancement from a randomly roughened back reflector ( $\sim 50$ ).

The optimized solar cell with the photonic crystal can achieve absorption considerably larger than that without the photonic crystal (Fig. 3.7). Most of the enhanced absorption (Fig. 3.7a, b) occurs near the band edge (600 – 775 nm), where photons have long absorption lengths. The photonic crystal generates modes of diffraction at these wavelengths, effectively increasing the path length or dwell time. We use the observed absorption, and wavelength-dependent absorption length of a-Si:H, to extract an optical path length of photons in the absorber layer. The ratio of the optical path length to the thickness of the absorber (Fig. 3.7c), is a convenient figure of merit. The theoretical limit of light path length enhancement from randomly roughened back reflector is about  $4n^2$ , where  $n$  is the refractive index of the absorber layer.<sup>12</sup> This predicts an enhancement of absorption of  $\sim 50$  for silicon thin films. However this assumes that the textured back reflector is loss-less, which is not the case in practice. Springer et al measured losses of 3 – 8% at the textured back reflector with each reflection from excitation of surface plasmon modes at the interface.<sup>2</sup> This reduces the observed optical path length enhancement to much less than 50. The best enhancement of  $\sim 10$  has been estimated in solar cells with roughened metallic interfaces.<sup>13</sup> Compared with the common textured back reflector, the 2D photonic crystal grating can achieve much greater enhancement around several hundred at resonance wavelengths (Fig. 3.7c), and exceeding the theoretical limit for the random diffusive optical scattering (Fig 3.7c) for most wavelengths near the band edge. The purely dielectric PC and DBR, should not exhibit losses associated with metallic components. Below 600 nm, the photonic crystal has little effect, since photons have absorption lengths smaller than the film thickness and are effectively absorbed within the a-Si:H absorber layer, without reaching the back surface. The fall-off in the absorption at short wavelengths is due to the high absorption of the p-layer.

## Discussion and Conclusions

We have also examined an alternative photonic crystal configuration where the PC resides between the antireflective coating and the absorber. The disadvantage of this front grating design is that the photonic crystal contains p-type a-Si:H. Such a thick p-layer is highly ab-

sorptive and the carriers created within this p-layer can not be collected by the solar cell. A thick p-layer degrades the short circuit current, as we have confirmed with Analysis of Micro-electronic and Photonic Structures (AMPS) device simulations. The back grating studied in this paper may utilize n-type a-Si:H within the PC. The absorption within the n-layer is low. Thicker n-layers have little effect on the short circuit current.

Plasmon-assisted schemes, where metal nanoparticles have surface plasmon resonances that concentrate light field, can also provide promising absorption improvements in a-Si:H solar cells.<sup>14,15</sup> They may be an alternative to the photonic crystal concept presented here.

The optimized photonic crystal has a lattice constant of  $0.7 \mu m$ , and the performance decreases for larger spacing (Fig. 3.5). Fabrication of such a small pitch ITO photonic crystal on large areas is certainly challenging. A viable approach is using holographic lithography, where interference between two or more coherent light beams can produce a periodic intensity pattern.<sup>16,17</sup> It has been shown that by varying the angle of the beams and exposure times, a variety of high symmetry lattice structures with periods less than  $1 \mu m$  were produced on semiconductor substrates covered with photoresist.<sup>18</sup> Such holographically generated patterns with periods less than  $1 \mu m$  have already been utilized to enhance the light extraction of light-emitting diodes.<sup>18</sup> Once a small area sample is synthesized, it can be repeated over a much larger area to obtain patterned areas suitable for large area solar cells. Finally, the periodic patterns are transferred to ITO using reactive ion etching. Sub-micron diffractive gratings<sup>19</sup> are clearly an aspect for future experimental work.

In conclusion, we develop a novel light trapping scheme in a-Si:H solar cells with dielectric photonic crystals. By combining a 2D PC diffraction grating and DBR, we can efficiently harvest solar photons, without losses associated with textured metallic reflectors. The photonic crystal provides loss-less diffraction of photons, increasing the photon path length within the absorber layer. For near band-edge photons with wavelength of  $600 - 775 nm$ , the optimized solar cells demonstrate more than hundred times increase in path length at diffraction resonances and exceed the classical light path enhancement limit predicted for randomly roughened interfaces. Such photonic crystal schemes can be extended to multi-junction cells. The en-



hancement is more profound for thinner cells. Since holes can be collected more efficiently for thinner cells, we can make even thinner and more efficient a-Si:H solar cells with the 2D PC and DBR.

## Acknowledgements

We acknowledge support from the Catron Solar Foundation. The Ames Laboratory is operated for the Department of Energy by Iowa State University under contract No. W-7405-Eng-82. We thank V. Dalal for many stimulating discussions and C. G. Ding for the computational codes. We also acknowledge partial support from the NSF under grant ECS-06013177. We thank R. Collins and N. Podraza for kindly supplying the optical data for amorphous silicon films and most helpful discussions.

## References

- <sup>1</sup>B. Yan, J. M. Owens, C. Jiang, J. Yang and S. Guha, *Proceedings of the 2005 Materials Research Society Symposia* (Materials Research Society, Pittsburgh, 2005), Vol. 862, p. 603.
- <sup>2</sup>J. Springer, A. Poruba, L. Mullerova, M. Vanecek, O. Kluth and B. Rech, *J. Appl. Phys.* **95**, 1427 (2004).
- <sup>3</sup>A. S. Ferlauto, G. M. Ferreira, J. M. Pearce, C. R. Wronski, R. W. Collins, X. Deng and G. Ganguly, *J. Appl. Phys.* **92**, 2424 (2002).
- <sup>4</sup>J. D. Joannopoulos, R. D. Meade and J. N. Winn, *Photonic Crystals* (Princeton University Press, Princeton, NY, 1995).
- <sup>5</sup>L. Zeng, Y. Yi, C. Hong, J. Liu, N. Feng, X. Duan, L. C. Kimmerling and B. A. Alamariu, *Appl. Phys. Lett.* **89**, 111111 (2006); *Proceedings of the 2005 Materials Research Society Symposia* (Materials Research Society, Pittsburgh, 2005), Vol. 862, p. 381.
- <sup>6</sup>P. Bermel, C. Luo and J. D. Joannopoulos, *Opt. Express* **15**, 16986 (2007)
- <sup>7</sup>R. Biswas and D. Zhou, *Proceedings of the 2007 Materials Research Society Symposia* (Materials Research Society, Pittsburgh, 2007), Vol. 989, p. A03.02.

- <sup>8</sup>Y. Fink, J. N. Winn, S. Fan, C. Chen, J. Michel, J. D. Joannopoulos and E. L. Thomas, *Science* **282**, 1679 (1998).
- <sup>9</sup>R. Biswas, C. G. Ding, I. Puscasu, M. Pralle, M. McNeal, J. Daly, A. Greenwald and E. Johnson, *Phys. Rev. B* **74**, 045107 (2006).
- <sup>10</sup>Z. Y. Li and L. L. Lin, *Phys. Rev. E* **67**, 046607 (2003).
- <sup>11</sup>ASTMG173-03, Standard Tables for Reference Solar Spectral Irradiances, (ASTM International, West Conshohocken, Pennsylvania, 2005).
- <sup>12</sup>E. Yablonovitch, *J. Opt. Soc. Am.* **72**, 899 (1982).
- <sup>13</sup>J. Nelson, *The Physics of Solar Cells* (Imperial College Press, London, 2003), p. 279.
- <sup>14</sup>D. Derkacs, S. H. Lim, P. Matheu, W. Mar, and E. T. Yu, *Appl. Phys. Lett.* **89**, 093103 (2006).
- <sup>15</sup>S. Pillai, K. R. Catchpole, T. Trupke, and M. A. Green, *J. Appl. Phys.* **101**, 093105 (2007).
- <sup>16</sup>V. Berger, O. GauthierLafaye and E. Costard, *J. Appl. Phys.* **82**, 60 (1997).
- <sup>17</sup>H. H. Solak, C. David, J. Gobrecht, V. Golovkina, F. Cerrina, S. O. Kim and P. F. Nealey, *Microelectron. Eng.* **67**, 56 (2003).
- <sup>18</sup>D.-H. Kim, C.-O. Cho, Y.-G. Roh, H. Joen, Y. S. Park, J. Cho, J. S. Im, C. Sone, Y. Park, W. J. Choi and Q.-H. Park, *Appl. Phys. Lett.* **87**, 203508 (2005).
- <sup>19</sup>K. R. Catchpole and M. A. Green, *J. Appl. Phys.* **101**, 063105 (2007)

## CHAPTER 4 GENERAL CONCLUSIONS

### General Discussion

In this work, we develop a novel light-trapping scheme in a-Si:H solar cells with the combination of 2D photonic crystals and DBR. The dielectric pairs forming the photonics crystals and DBR can be Si/SiO<sub>2</sub> and Si/ITO. The Si/SiO<sub>2</sub> combination can provide stronger diffraction and high reflectivity DBR with less pairs, while the Si/ITO combination have the advantage that the DBR can be made conductive and used as back contact. In both the combinations, the photonic crystal can increase the photon path length within the absorber layer. Simulations show that the path length enhancement can reach several hundred times at diffraction resonance and far exceed the classical light path length enhancement limit predicted for randomly textured surfaces. Since the enhancement is more profound for thinner cells, we can make thinner and more efficient a-Si:H solar cells.

We have also examined an alternative front grating, where the PC resides between the anti-reflective coating and the absorber. The simulations show that same level of path length enhancement can be obtained in this structure, but there are some precautions in making those devices. Since a p-layer is highly absorptive and the carriers generated within can not be collected by the contacts, a thick p-layer should be avoided. For this reason, the holes in the top ITO should not be filled entirely with p-type silicon. Instead, a thin layer of p-type silicon ( $\sim 20$  nm) should be deposited conformally.

The optimized photonic crystal has a lattice constant of  $\sim 0.7$   $\mu$ m. With R/a ratio  $\sim 0.4$ , the smallest feature size is on the order of 140 nm. It is certainly a challenge to fabricate photonic crystal with such a small pitch size on larger areas. A popular alternative to the standard photolithography is electron-beam lithography (E-beam lithography). Various pho-

tonic crystals can be created with extremely high resolution. Due to its complexity, the cost of the E-beam lithography is high and not suitable for mass production of solar cells.

Thanks to the periodic nature of photonic crystals, a viable solution is to use interference lithography (holographic lithography), where interference between two or more coherent light beams can produce a periodic intensity pattern [1, 2]. By splitting the initial laser beam, several coherent beams can be generated and overlap on the photoresist at angles. It has been shown that by varying the angle of the beams and exposure times, a variety of high symmetry lattice structures with periods less than 100 *nm* can be produced on semiconductor substrate covered with photoresist [3]. Once a small area sample is synthesized, it can be repeated over a much larger area to obtain patterned areas suitable for large area solar cells. The holographic lithography technique has already been successfully utilized to enhance the light extraction of light-emitting diodes. 2D square lattice photonic crystals with period from 300 - 700 *nm* can be fabricated on large areas with high throughput [4]. Among the competing technologies, nanoimprint lithography is another alternative for high throughput and low cost production. In an imprint process, a mold with nanostructure formed on the surface is pressed into photoresist on a substrate. Structures with feature size of 25 *nm* have been demonstrated [1]. After periodic patterns are formed on the photoresist, they can be transferred to ITO using reactive ion etching. Fabrication of the structure we suggested is an aspect for further experimental work.

## Recommendations for Future Research

In light of the recent development of plasmonics, plasmon-assisted light-trapping schemes have attracted much attention [5, 6]. It has been shown that localized surface plasmon on metallic nanoparticle can concentrate light field and couple light into and out of dielectric waveguide efficiently. We also run some preliminary simulations on free standing periodic gold nanoparticle arrays. For triangular lattice of gold cylinder array with lattice constant of 1  $\mu m$ , the height of the cylinder is 60 *nm*. The  $R/a$  ratios vary from 0.05 to 0.11, corresponding to cylinder diameter of 100 to 220 *nm*. The absorption in the nanoparticle arrays with different

radius is below 5% at most wavelengths (Fig. 4.1a). The diffraction is measured as difference between the non-specular and the specular transmission (Fig 4.1b). The diffraction is minimized at Wood's anomaly wavelengths, which can be predicted by the following equation [8],

$$\lambda_{mn} = \frac{2\pi}{G_{mn}} = \frac{a}{\sqrt{m^2 + (2n - m)^2/3}} \quad (4.1)$$

where  $G_{mn}$  is the reciprocal lattice vector of the triangular lattice. Also, there is no diffraction beyond  $a\sqrt{3}/2$ .

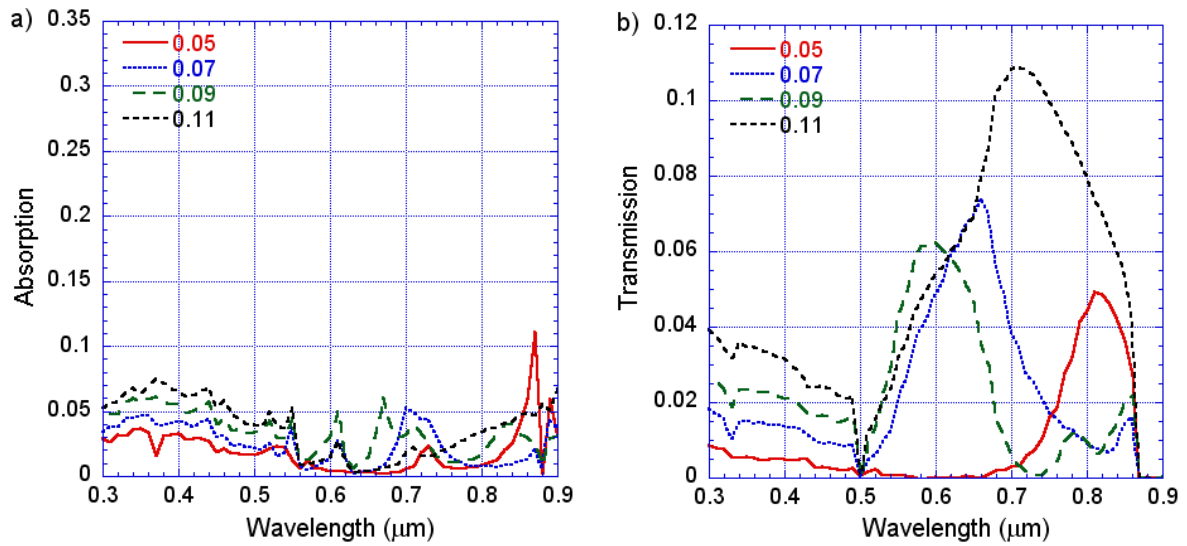


Figure 4.1 a) The absorption and b) The diffraction in the gold nanoparticle array with  $a = 1 \mu m$ ,  $d = 60 nm$  and  $R/a$  of 0.05, 0.07, 0.09 and 0.11.

As we can see from figure 4.1, in some wavelength ranges, the gold nanoparticle array can provide strong diffraction with minimal absorption. They can make good candidates for light-trapping in thin film solar cells. The absorption and diffraction by gold nanoparticle array residing on dielectric substrates are more complicated. With careful design, this plasmon-assisted light-trapping scheme is very promising.

## References

1. V. Berger, O. Gauthier Lafaye and E. Costard, J. Appl. Phys. **82**, 60 (1997).

2. Paras N. Prasad, *Nanophotonics* (Wiley-Interscience, Hoboken, New Jersey, 2004).
3. H. H. Solak, C. David, J. Gobrecht, V. Golovkina, F. Cerrina, S. O. Kim and P. F. Nealey, *Microelectronic Engineering* **67**, 56 (2003).
4. D.-H. Kim, C.-O. Cho, Y.-G. Roh, H. Joen, Y. S. Park, J. Cho, J. S. Im, C. Sone, Y. Park, W. J. Choi and Q.-H. Park, *Appl. Phys. Lett.* **87**, 203508 (2005).
5. D. Derkacs, S. H. Lim, P. Matheu, W. Mar, and E. T. Yu, *Appl. Phys. Lett.* **89**, 093103 (2006).
6. S. Pillai, K. R. Catchpole, T. Trupke, and M. A. Green, *J. Appl. Phys.* **101**, 093105 (2007).
7. K.R. Catchpole, and S. Pillai, *Journal of Luminescence* **121**, 315 (2006).
8. R. Biswas, S. Neginhal, C. G. Ding, I. Puscasu and E. Johnson, *J. Opt. Soc. Am. B.* **24**, 2589 (2007).

## ACKNOWLEDGEMENTS

I would like to take this opportunity to express my thanks to those who helped me with various aspects of conducting research and the writing of this thesis.

First and foremost, my major professor, Dr. Rana Biswas, for his guidance and support throughout this research and the writing of this thesis. Dr. Gary Tuttle and Dr. Jiming Song for being excellent teachers and resources and for serving on my POS committee. Dr. Vikram Dalal for valuable suggestions and for serving on my POS committee. Jane Woline and Pam Myers for their administrative support.

I also would like to thank Max Noack, Daniel Stieler and many other friends and colleagues at Microelectronics Research Center for their technical support on fabrication.